
CardioGenAI: A Machine Learning-Based Framework for Re-Engineering Drugs for Reduced hERG Liability

Gregory W. Kyro^{1,*}, Matthew T. Martin², Eric D. Watt², Victor S. Batista^{1,*}

¹Department of Chemistry, Yale University, New Haven, Connecticut 06511

²Drug Safety Research & Development, Pfizer Worldwide Research, Groton, Connecticut 06340

*Correspondence to {gregory.kyro, victor.batista}@yale.edu

Abstract

Drug-induced cardiotoxicity is a major health concern which can lead to serious adverse effects including life-threatening cardiac arrhythmias via the blockade of the voltage-gated hERG potassium ion channel. It is therefore of tremendous interest to develop advanced methods to identify hERG-active compounds in early stages of drug development, as well as to optimize commercially available drugs for reduced hERG activity. In this work, we present CardioGenAI, a machine learning-based framework for re-engineering both developmental and marketed drugs for reduced hERG activity while preserving their pharmacological activity. The framework incorporates novel state-of-the-art discriminative models for predicting hERG channel activity, as well as activity against the voltage-gated Nav1.5 and Cav1.2 channels due to their potential implications in modulating the arrhythmogenic potential induced by hERG channel blockade. These models can also serve independently as effective components of a virtual screening pipeline. We applied the complete framework to pimozide, an FDA-approved antipsychotic agent that demonstrates high affinity to the hERG channel, and generated 100 refined candidates. Remarkably, among the candidates is fluspirilene, a compound which is of the same class of drugs (diphenylmethanes) as pimozide and therefore has similar pharmacological activity, yet exhibits over 700-fold weaker binding to hERG. We have made all of our software open-source to facilitate integration of the CardioGenAI framework for molecular hypothesis generation into drug discovery workflows.

1. Introduction

Drug-induced cardiotoxicity due to the blockade of the voltage-gated $K_v11.1$ potassium ion channel is a major health concern and continues to cause serious adverse reactions in many commercially available drugs.¹ Moreover, the pharmaceutical industry incurs substantial financial and developmental setbacks from cardiotoxicities identified during early, preclinical and clinical phases of drug development.²

The International Council for Harmonisation of Technical Requirements for Pharmaceuticals for Human Use (ICH) sets forth guidelines to evaluate the potential for compounds to induce arrhythmias (e.g., Torsade de Pointes) via blockade of the $K_v11.1$ channel. Each functional unit of this channel is a homo-tetramer of α protein subunits, each of which is encoded by the human Ether-à-go-go-Related Gene (hERG; *KCNH2* gene).^{3, 4} The hERG channel opens in response to depolarization of the cell membrane, selectively allowing potassium ions to flow out of the cell, thereby facilitating the restoration of the cell's membrane potential to its resting state (i.e., repolarization).⁵ Inhibition of this channel can therefore disrupt cardiac repolarization, leading to prolongation of the cardiac action potential and an increased risk of arrhythmias.¹

The Comprehensive In Vitro Proarrhythmia Assay (CiPA) initiative,⁶ supported by regulatory agencies including the U.S. Food and Drug Administration (FDA), established guidelines that also incorporate the voltage-gated sodium ($Na_v1.5$) and calcium ($Ca_v1.2$) ion channels alongside the hERG channel due to their critical roles in initiating and sustaining the cardiac action potential and their relevance to the development of arrhythmias.⁷ Previous work indicates that modulating $Na_v1.5$ and $Ca_v1.2$ channel activities can mitigate the arrhythmogenic potential induced by hERG channel blockade.^{8, 9} Therefore, it is of tremendous interest to develop highly capable methods for assessing how both prospective and currently available drugs interact with each of these three channels.

A multitude of experimental methods exist for in vitro determination of cardiac ion channel affinity.¹⁰⁻¹³ However, they are generally time-consuming and expensive, rendering them unsuitable for large-scale compound screening. Machine learning (ML)-based in silico methods for predicting hERG channel activity have been extensively explored, utilizing both protein structure-based and ligand-based models.¹⁴⁻³⁸ These methods are significantly cheaper and much faster than experimental methods, and are applicable to large-scale virtual screening in hit identification. However, structure-based predictive modeling of the hERG channel has proven to be difficult due to the channel's intricate structure, its dynamic nature encompassing multiple conformations, and the possibility of unexpected interaction sites that are not apparent in conventional structural models.³⁹ For these reasons, ligand-based methods currently predominate. Predictive modeling for $Na_v1.5$ and $Ca_v1.2$ channel blocking is comparatively unexplored, as the amount of available data is much less compared to that for hERG. However, recent benchmarks for predicting $Na_v1.5$ and $Ca_v1.2$ channel activity have been established,⁴⁰ and increasing effort is being devoted to developing models for these channels as well.⁴¹⁻⁴⁴

While ML-based discriminative models for predicting hERG channel blockers have tremendous potential for applications in virtual screening, extending these capabilities to de novo design

through generative artificial intelligence can overcome the constraints of the currently available molecular libraries by enabling the direct in silico development of drugs with desired chemical properties and activity against cardiac ion channels. Furthermore, numerous generative models have already demonstrated the ability to produce valid molecules with prespecified drug-like properties.⁴⁵⁻¹⁰⁴ However, this approach would still necessitate subsequent virtual screening to identify hit compounds from a vast search space, requiring a significant amount of additional resources. To address this challenge, the space can be further constrained by utilizing a drug with a known pharmacological profile as a starting point for a search algorithm, and refining this drug to minimize hERG liability while retaining its therapeutic efficacy.

In this work, we present an ML-based framework designed to re-engineer both developmental and commercially available drugs for reduced hERG liability while preserving their pharmacological activity. The method utilizes a generative model to produce molecules conditioned on the molecular scaffold and absorption, distribution, metabolism, excretion, and toxicity (ADMET) properties of the input hERG-active molecule. The generated ensemble is filtered using deep learning models for predicting hERG, Nav1.5 and Cav1.2 channel activity. A chemical space representation is then constructed from the filtered generated distribution and the input molecule, where nearby molecules exhibit similar chemical properties, thus facilitating the identification of molecules with similar pharmacological activity to the input molecule but with reduced hERG channel inhibition. This approach, while not a replacement for the expertise of medicinal chemists, is highly effective at rapid molecular hypothesis generation, proposing refined candidates that can then be investigated with more expensive computational methods and experimental techniques.

2. Overview of CardioGenAI Framework

The CardioGenAI framework combines generative and discriminative ML models to re-engineer cardiotoxic compounds for reduced hERG channel inhibition while preserving their pharmacological action. An autoregressive transformer is trained on a dataset that we previously curated which contains approximately 5 million unique and valid SMILES strings derived from ChEMBL 33, GuacaMol v1, MOSES, and BindingDB datasets.¹⁰⁵⁻¹⁰⁹ The model is trained autoregressively, receiving a sequence of SMILES tokens as context as well as the corresponding molecular scaffold and ADMET properties, and iteratively predicting each subsequent token in the sequence. Once trained, this model is able to generate valid molecules conditioned on a specified molecular scaffold along with a set of ADMET properties. For an input hERG-active compound, the generation is conditioned on the scaffold and ADMET properties of this compound (Figure 1A). Each generated compound is subject to filtering based on activity against hERG, Nav1.5 and Cav1.2 channels. Depending on the desired activity against each channel, the framework employs either classification models to include predicted non-blockers or regression models to include compounds within a specified range of predicted pIC50 values. Both the classification and regression models utilize the same architecture, and are trained using three feature representations of each molecule: a feature vector that is extracted from a bidirectional transformer trained on SMILES strings, a molecular fingerprint, and a graph (more details in section 3.1). For each molecule in the filtered generated ensemble and the input hERG-active molecule, a feature vector

is constructed from the 209 chemical descriptors available through the RDKit Descriptors module.¹¹⁰ The redundant descriptors are then removed according to pairwise mutual information calculated for every possible pair of descriptors. Cosine similarity is then calculated between the processed descriptor vector of the input molecule and the descriptor vectors of every generated molecule to identify the molecules most chemically similar to the input molecule, but with desired activity against each of the cardiac ion channels (Figure 1B).

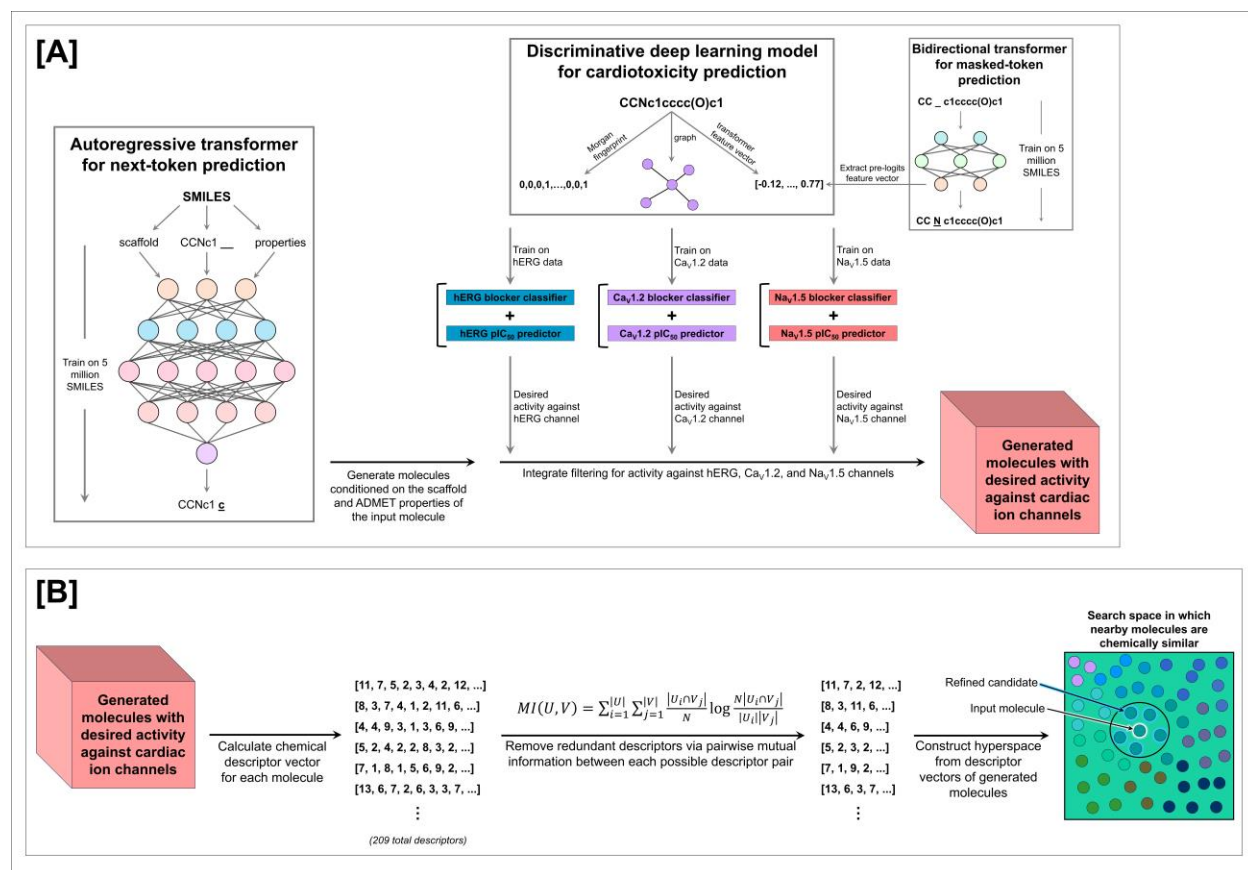


Figure 1. CardioGenAI framework for re-engineering hERG-active compounds. An autoregressive transformer is trained on approximately 5 million unique and valid SMILES strings derived from ChEMBL 33, GuacaMol v1, MOSES, and BindingDB databases for next-token prediction, conditioned on a molecular scaffold and a set of ADMET properties. For a given input molecule, the generation is conditioned on the scaffold and ADMET properties of this molecule. Generated molecules are filtered based on desired activity against hERG, Nav1.5 and Cav1.2 channels, as shown in [A]. For each generated molecule, as well as the input molecule, a chemical descriptor vector is calculated, and the redundant descriptors among the set of all molecules are removed according to pairwise mutual information between every possible descriptor pair. Cosine similarities are then calculated between the descriptor vector of the input molecule and every other descriptor vector to identify the most chemically similar molecules to the input molecule but with desired activity against the cardiac ion channels, as shown in [B].

3. Discriminative Models for Predicting Cardiac Ion Channel Activity

3.1. Data Featurization

For training and evaluation of hERG, Nav1.5 and Cav1.2 activity prediction models, we utilize the training and evaluation datasets included in the benchmarks recently developed by Arab et al.⁴⁰ These benchmarks are designed to assess model generalizability, enforcing a maximum fingerprint similarity cutoff between molecules in the training and evaluation sets. Multiple published models in the field have been assessed using evaluation sets that have significant overlap with the corresponding training sets,^{37, 111} undoubtedly yielding overoptimistic results with respect to the models' abilities to generalize. The compounds in the evaluation sets used in this work have a structural similarity, as determined by pairwise Tanimoto similarity between 2048-bit Morgan fingerprints, no greater than 0.70 to any compound in the corresponding training or validation sets. Compounds were sourced from the ChEMBL bioactivity database,¹¹²⁻¹¹⁴ PubChem,¹¹⁵ BindingDB,^{109, 116} hERGCentral,¹¹⁷ and the scientific literature.^{37, 118-120} Each molecule is represented as a SMILES string which was canonicalized using RDKit, and labeled with the experimentally determined cardiac ion channel pIC50 value. For binary classification tasks, compounds with a pIC50 value greater than or equal to 5.0 are labeled as blockers. For more details regarding the curation of the datasets, we refer readers to the original paper.⁴⁰

We find there to be a noteworthy positive correlation between pIC50 values and the logarithm of the partition coefficient between n-octanol and water (logP), as well as a negative correlation with topological polar surface area (TPSA) (Figure S1 in the *Supporting Information*). We also identify a relation between pIC50 values and the presence of charged nitrogen atoms within aromatic or hydrophobic groups among the molecules exhibiting the most substantial hERG activity (Figure S2 in the *Supporting Information*).

We represent each compound as three distinct forms: a 256-dimensional feature vector that is extracted from a bidirectional transformer trained on SMILES strings, a 1024-bit Extended-Connectivity Fingerprint with a radius of 2 bonds (ECFP2) generated using the Morgan algorithm, and a graph (Figure 2). A bidirectional transformer is first trained for masked-token prediction on the same dataset used to train the autoregressive transformer, allowing it to develop an intricate internal representation of molecular structure and grasp the syntax of SMILES notation (more details in section 4.1). After this model is fully trained, it is used as a means of extracting a context-rich feature vector as a representation of a given SMILES string (more details in section 4.2). Specifically, the processed vector from the penultimate layer of the model corresponding to the start token is extracted, containing information about the entire SMILES string that contributes to the prediction of a masked token within the sequence. This information encapsulates nuanced inter-token relationships and patterns among different molecules, rendering this feature vector a powerful representation that captures important characteristics of the molecule in a high-dimensional space. In the graph representation, nodes are atoms and edges are bonds. Each node is represented as a 14-dimensional vector of atomic features: carbon indicator, nitrogen indicator, oxygen indicator, phosphorous indicator, sulfur indicator, hydrophobicity indicator, aromaticity indicator, hydrogen bond acceptor indicator, hydrogen bond donor indicator, ring structure

indicator, number of bonds to heavy atoms, number of bonds to heteroatoms, partial charge, and atomic mass. Each edge has two features: bond order and aromaticity indicator.

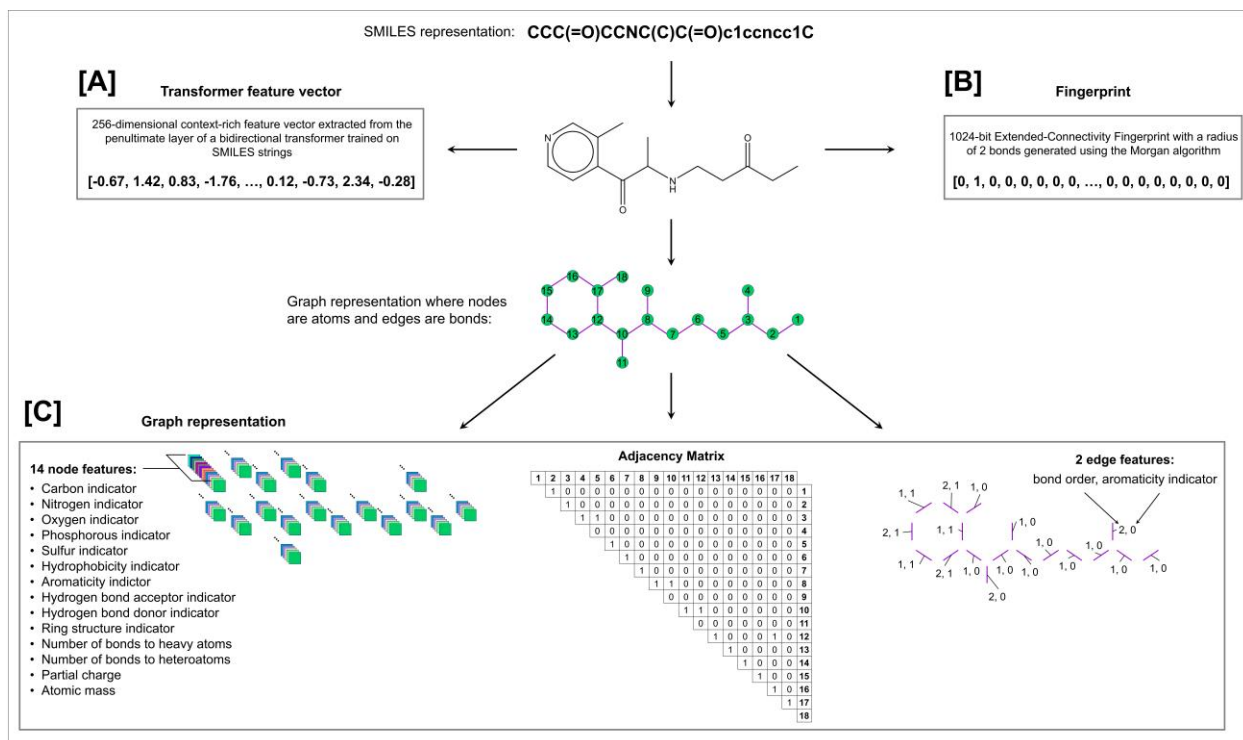


Figure 2. Featurization of a SMILES string for use by the cardiac ion channel activity prediction models. Each SMILES string is represented as [A] a 256-dimensional feature vector that is extracted from the penultimate layer of a bidirectional transformer trained on SMILES strings, [B] a 1024-bit Extended-Connectivity Fingerprint with a radius of 2 bonds generated using the Morgan algorithm, and [C] a graph.

3.2. Model Architecture

The transformer-based feature vector and the ECFP2 are each processed by separate two-layer feed-forward networks (Figure 3B,C). For each of the two layers of the networks, the input vector undergoes a linear transformation followed by batch normalization. The normalized output is then passed through a ReLU activation function, followed by dropout with a rate of 50%. The graph representation is processed by a graph attention network (GAT) consisting of two GAT convolutional layers (Figure 3A). Initially, the graph is augmented with self-loops to ensure that each node's feature vector is included in its own neighborhood during feature aggregation. The first GAT layer transforms the node feature vectors through a linear operation, followed by a softmax-based attention mechanism to assign weights to the features of each node's neighbors. The output of this layer is passed through a ReLU activation function and fed to the second GAT convolutional layer which operates analogously to the first layer. After being processed by the second GAT convolutional layer, the updated node features are aggregated to form a graph-level representation using a global add pooling operation, which sums the node features across all nodes

to generate a single vector that encapsulates the entire graph’s information. After each of the three input feature representations has been encoded, they are concatenated to form a combined feature vector. This combined feature vector is then passed through a two-layer feed-forward network (Figure 3D). The first layer applies a linear transformation to the feature vector followed by batch normalization. The normalized output is then passed through a ReLU activation function followed by dropout with a rate of 50%. The output of this layer then undergoes a linear transformation to map it to the final output space.

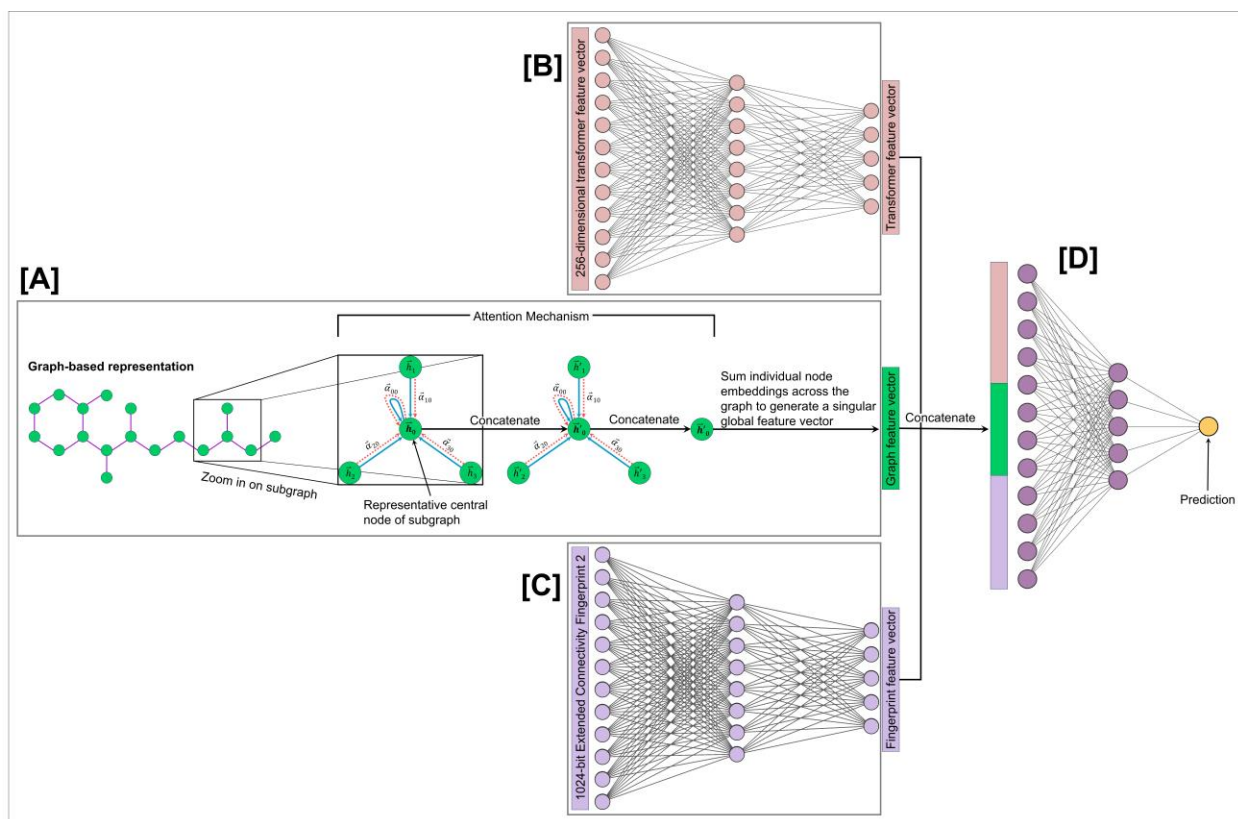


Figure 3. Forward pass of the cardiac ion channel activity prediction models. The graph representation of a given SMILES string is encoded by [A] a graph attention network. The [B] transformer-derived and [C] fingerprint feature vectors are encoded by feed-forward networks. These three encodings are then concatenated and passed to [D] a final feed-forward network to generate a prediction.

3.3. Trainings and Hyperparameters

The classification and regression models for each cardiac ion channel were trained for 100 epochs with a batch size of 32. The AdamW optimizer, a variant of the Adam optimizer that incorporates weight decay for regularization, was used with a learning rate of 3×10^{-4} and a weight decay of 1×10^{-4} to optimize the models’ parameters. Additionally, L1 regularization was applied with a regularization coefficient of 1×10^{-4} to induce sparsity within the model parameters. We integrate a learning rate scheduler which monitors the training loss and halves the learning rate if no

improvement is observed for 10 consecutive epochs. To ensure stability in training and prevent gradient explosion, gradient clipping was applied with a maximum norm of 5.0. For the classification and regression models, binary cross entropy loss and mean squared error loss were used as objective functions, respectively. The model parameters used for inference are those from the epoch with the highest validation accuracy for classification and highest validation Pearson correlation for regression. Learning curves for each of the classification and regression models are reported in Figure S3 of the *Supporting Information*).

3.4. Benchmarking Against Existing Models

We compare the performance of our cardiac ion channel classification models to the highest-performing models in the literature that have been evaluated with the benchmarks used in this work. Computed metrics include accuracy $\left(\text{AC} = \frac{TP+TN}{TP+TN+FP+FN}\right)$, sensitivity $\left(\text{SN} = \frac{TP}{TP+FN}\right)$, specificity $\left(\text{SP} = \frac{TN}{TN+FP}\right)$, F1-score $\left(\text{F1} = \frac{TP}{TP+\frac{1}{2}(FP+FN)}\right)$, correct classification rate $\left(\text{CCR} = \frac{SN+SP}{2}\right)$, and Matthew’s correlation coefficient $\left(\text{MCC} = \frac{TP \times TN - FP \times FN}{\sqrt{(TP+FP) \times (TP+FN) \times (TN+FP) \times (TN+FN)}}\right)$, where TP , TN , FP , and FN represent the number of true positives, true negatives, false positives, and false negatives, respectively. We find that our model outperforms the existing models in the literature on the hERG benchmark for binary classification (Table 1). Additionally, we assess our model with different combinations of feature representations, and find that utilizing all three (i.e., transformer-based feature vector, fingerprint, and graph) achieves the best performance on the hERG benchmark (Table S4 in the *Supporting Information*).

Table 1. Performance of CardioGenAI for binary classification of hERG channel blockers compared to the highest-performing models in the literature.

Model	AC	SN	SP	F1	CCR	MCC
CardioGenAI	83.5	86.2	80.3	85.1	83.2	66.7
CToxPred-hERG	81.4	86.7	74.6	83.9	80.7	62.1
CardioTox	81.2	83.0	78.9	83.1	81.0	61.9
ADMETlab 2.0	71.7	71.6	71.8	73.8	71.7	43.1
ADMETsar 2.0	68.5	84.5	48.3	75.0	66.4	35.5
CardPred	56.1	52.7	60.3	57.0	56.5	13.0

^a Compounds in the evaluation set have a structural similarity, as determined by pairwise Tanimoto similarity between 2048-bit Morgan fingerprints, no greater than 0.70 to any compound in the corresponding training or validation sets.

^b The top value achieved for each metric is shown in bold.

^c Accuracy (AC), sensitivity (SN), specificity (SP), F1-score (F1), correct classification rate (CCR), and Matthew's correlation coefficient (MCC) are shown.

^d Results are shown for CToxPred-hERG,⁴⁰ CardioTox,³² ADMETlab 2.0,¹²¹ ADMETsar 2.0,¹²² and CardPred.²⁰

For the Nav1.5 and Cav1.2 benchmarks, only the models presented by Arab et al.⁴⁰ have been evaluated, largely owing to the fact that the experimental data available for these channels are scarce compared to those for hERG, and these benchmarks have only recently been developed. We find that our models demonstrate superior performance for both channels (Table 2). Additionally, the area under the curve (AUC) of the receiver operating characteristic for each channel is commensurate with the accuracy that our models obtain; hERG AUC is 0.88, Nav1.5 AUC is 0.89, and Cav1.2 AUC is 0.95 (Figure S5B in the *Supporting Information*). We also calculate the Pearson correlation between true pIC50 values and those predicted by our regression models, and obtain correlation coefficients of 0.67 for hERG, 0.60 for Nav1.5, and 0.81 for Cav1.2 benchmarks (Figure S5C-E in the *Supporting Information*).

Table 2. Performance of CardioGenAI for binary classification of Nav1.5 and Cav1.2 blockers compared to that of the models presented by Arab et al.⁴⁰

Channel	Model	AC	SN	SP	F1	CCR	MCC
Nav1.5	CardioGenAI	89.4	95.9	75.6	92.5	85.7	75.1
	CToxPred-Nav	81.7	85.6	73.3	86.5	79.5	58.2
Cav1.2	CardioGenAI	91.4	96.2	82.8	93.5	89.5	81.0
	CToxPred-Cav	86.4	96.2	69.0	90.1	82.6	70.2

^a Compounds in the evaluation set have a structural similarity, as determined by pairwise Tanimoto similarity between 2048-bit Morgan fingerprints, no greater than 0.70 to any compound in the corresponding training or validation sets.

^b The top value achieved for each metric is shown in bold.

^c Accuracy (AC), sensitivity (SN), specificity (SP), F1-score (F1), correct classification rate (CCR), and Matthew's correlation coefficient (MCC) are shown.

3.5. Application to DrugCentral Database of FDA-Approved Drugs

To demonstrate the practical utility of our classification and regression models, we applied them to the FDA-approved drugs from the DrugCentral database, offering a real-world context for assessing hERG channel inhibition.^{123, 124} Of the 1692 unique FDA-approved drugs, we classify 504 (29.8%) to be hERG blockers, 764 (45.2%) to be Nav1.5 blockers, and 400 (23.6%) to be Cav1.2 blockers (Figure S6A in the *Supporting Information*). A rigorous analysis of the cardiac ion channel activity of the FDA-approved drugs is reported in Figure S6B of the *Supporting Information*. In addition, we report the compounds with a predicted hERG pIC50 greater than 7.0 (i.e., more than 100-fold greater hERG inhibitory potency than the blocker threshold) in Table 3.

For the 11 FDA-approved compounds with a predicted hERG pIC50 value greater than 7.0, the predicted pIC50 values correlate closely with those that are experimentally determined, with notable agreement in cases where the drug is not in the training set of the model (Table 3). The primary mechanism of action for three of the 11 drugs is to block the hERG channel: ibutilide,¹²⁵ dofetilide,¹²⁶ and amiodarone.¹²⁷ Another three of them function primarily as dopamine D2 receptor antagonists: pimozide,¹²⁸ droperidol,¹²⁹ and haloperidol decanoate.¹³⁰ Pimozide is reported to cause cardiac action potential prolongation and ventricular arrhythmias due to hERG channel blockade with high specificity and affinity;¹³¹ droperidol is reported to cause Torsade de Pointes due to potent hERG channel blockade;¹³² haloperidol decanoate has been found to cause sudden death due to hERG channel blockade-induced cardiac action potential prolongation.¹³³

Another two of the 11 drugs function primarily as H₁-receptor antagonists: astemizole and terfenadine.^{134, 135} Both of these drugs were withdrawn from the market due to hERG blockade-induced cardiac arrhythmias.^{136, 137} Of the remaining three drugs of the 11, nintedanib is reported to cause side effects related to hERG channel blockade,¹³⁸ halofantrine is found to cause hERG blockade-induced cardiac action potential prolongation,¹³⁹ and tolterodine is reported to cause hERG blockade-induced tachycardia and palpitations.¹⁴⁰ These results support the real-world application of this model to hERG activity prediction.

Table 3. Analysis of the FDA-approved compounds with a predicted hERG pIC₅₀ greater than 7.0.

Drug Name	Pharmacological Indication	Mechanism of Action	FDA Approval Status	Predicted hERG Channel pIC ₅₀	In Training Set	Experimentally Determined pIC ₅₀
Nintedanib	Idiopathic pulmonary fibrosis	Kinase inhibitor	Approved	8.234	yes	8.585
Ibutilide	Atrial fibrillation, atrial flutter	hERG channel blocker	Approved	7.977	yes	8.000
Pimozide	Tourette's disorder	Dopamine D2 receptor antagonist	Approved	7.629	yes	8.520
Halofantrine	Severe malaria	Forms toxic complexes with ferritoporphyrin IX	Approved	7.588	no	7.398
Astemizole	Allergy symptoms	H ₁ -receptor antagonist	Withdrawn due to concerns of arrhythmias	7.562	yes	8.538
Tolterodine	Overactive bladder	Muscarinic receptor antagonist	Approved	7.311	no	7.886
Droperidol	Nausea and vomiting in surgical and diagnostic procedures	Dopamine D2 receptor antagonist	Approved	7.300	yes	7.495
Dofetilide	Atrial fibrillation, atrial flutter	hERG channel blocker	Approved	7.164	yes	8.194
Haloperidol decanoate	Schizophrenia, psychotic disorders, Tourette's disorder	Dopamine D2 receptor antagonist	Approved	7.149	no	6.921
Amiodarone	Recurrent ventricular fibrillation, recurrent hemodynamically unstable ventricular tachycardia	hERG channel blocker	Approved	7.127	yes	7.523
Terfenadine	Allergic rhinitis, hay fever, allergic skin disorders	H ₁ -receptor antagonist	Withdrawn due to concerns of arrhythmias	7.022	yes	7.252

^a Information regarding the pharmacological indication and mechanism of action for each drug is obtained from DrugBank.^{141, 142}

4. Transformer-Based Models

4.1. Data Preparation

The generative autoregressive transformer and the bidirectional transformer used for extracting features to be utilized by the discriminative models are both trained with a dataset that we previously curated by combining all of the unique and valid SMILES strings from ChEMBL 33, GuacaMol v1, MOSES, and BindingDB datasets.¹⁰⁵⁻¹⁰⁹ We removed SMILES strings containing infrequent tokens, as well as those containing more than 133 tokens. The remaining SMILES strings are then extended, if necessary, to a length of 133 using a padding token “<pad>”, and augmented with a start token “[CLS]” and an end token “[EOS]”. The processed dataset contains approximately 5.5 million SMILES strings which are randomly split into training (5 262 776 entries; 95%) and validation (276 989 entries; 5%) sets. Please refer to our previous paper for complete details regarding SMILES string preprocessing.¹⁰⁵

For each SMILES string, we calculate the molecular scaffold using the Murcko algorithm,¹⁴³ which identifies the core structure by removing side chains from the molecular graph, retaining the ring systems and the linkers connecting them. We also calculate ten ADMET properties for each SMILES string: molecular weight, number of rings, number of rotatable bonds, number of hydrogen bond donors, number of hydrogen bond acceptors, TPSA, number of heteroatoms, logP, number of stereocenters, and formal charge.

4.2. Model Architectures

For a given SMILES string, the autoregressive transformer considers the sequence of the SMILES string, the molecular scaffold, and the set of ADMET properties, while the bidirectional transformer only considers the sequence. For both models, tokens in the sequence are embedded using a learnable embedding table, where each token in the vocabulary corresponds to a learnable embedding vector. The positions of the tokens in the sequence are embedded using a separate learnable embedding table, where each index in the sequence corresponds to a learnable embedding vector that allows the model to account for a given token’s position in the sequence and capture sequential context within the SMILES string. For the autoregressive transformer, the set of ADMET properties is mapped to the embedding dimension via a learnable linear transformation, and the molecular scaffold is embedded using a learnable embedding table analogous to that used for the token embeddings. For both models, all embeddings, each with an embedding dimension of 256, are summed to create a combined feature representation, and then dropout is applied with a rate of 10%.

The transformer architectures consist of eight sequential blocks, each beginning with layer normalization to stabilize the input. This is followed by a self-attention mechanism, where query (Q), key (K), and value (V) vectors are computed for each input token, attention scores are derived via a scaled dot product of Q and K vectors, and softmax normalizes these scores to obtain weights that modulate the aggregation of V , effectively capturing the magnitude with which each token will attend to every other token in the sequence. The self-attention mechanism is executed multiple

times in parallel through what is known as multi-head attention. The models used in this work employ eight attention heads, where each head uses its own set of learned linear transformations to generate Q , K , and V vectors for each token in the sequence, allowing the model to simultaneously focus on different aspects of the input across the various heads. Representative attention maps for the bidirectional transformer and autoregressive transformer are reported in Figures S7 and S8 of the *Supporting Information*. The outputs of all attention heads are concatenated and passed through a learned linear transformation to generate the final output of the multi-head attention mechanism. A residual connection then merges this output with the initial block input. The resulting data tensor then undergoes another layer normalization and progresses through a two-layer feed-forward network with a 10% dropout rate and GeLU activation, before reintegration with its pre-normalized state. The final step involves another layer normalization, followed by a linear transformation that projects the data tensor onto the vocabulary space, generating a logits vector (i.e., the unnormalized log probabilities for each token in the vocabulary). When using the trained bidirectional transformer to derive feature vectors to be utilized by the discriminative models, the data tensor is extracted immediately prior to the final linear transformation, and the vector corresponding to the start token is used as the feature vector.

4.3. Trainings and Hyperparameters

The autoregressive transformer is trained for next-token prediction, and the bidirectional transformer is trained for masked-token prediction, where 15% of the tokens in a given SMILES sequence are randomly selected for masking; of these, 80% are replaced with a mask token “<MASK>”, 10% are replaced with a random token from the vocabulary, and the remaining 10% are left unchanged. Both models were trained for 100 epochs with a batch size of 512. The Sophia optimizer was used with a learning rate of 3×10^{-4} and a weight decay of 1×10^{-1} ,¹⁴⁴ and cross entropy loss was used as the objective function for both models. The model parameters used for inference are those from the last epoch of training. Learning curves for the autoregressive transformer and bidirectional transformer are reported in Figure S9 of the *Supporting Information*.

4.4. Molecular Generation

The autoregressive transformer is used to generate SMILES strings, conditioned on both a molecular scaffold and a set of ADMET properties. To rigorously evaluate the model’s ability to generate molecules with prespecified ADMET properties, we fix one ADMET property at a time to a discrete value while the other nine properties are sampled using a random uniform distribution within ranges of acceptable values based on ADMETlab 2.0 guidelines for medicinal chemistry.¹²¹ This procedure is performed for 500 molecules per fixed ADMET value. For example, we generate 500 molecules conditioned on a molecular weight of 400 and another 500 conditioned on a molecular weight of 600 to assess the model’s ability to generate molecules with a targeted molecular weight. We repeat this approach for each ADMET property, and observe that the model is able to successfully generate molecular distributions that satisfy the prespecified criteria (Figure S10A-I in the *Supporting Information*). We also demonstrate the model’s ability to generate

molecules conditioned on multiple discrete ADMET values simultaneously (e.g., TPSA of 50 and molecular weight of 350), validating its utility and justifying its use within the complete CardioGenAI framework (Figure S10J in the *Supporting Information*).

5. Complete CardioGenAI Framework

5.1 High-Level Description of the Workflow

The fundamental objective of the CardioGenAI framework is to re-engineer cardiotoxic compounds for reduced hERG channel activity while preserving their pharmacological action. Within the framework, the autoregressive transformer first generates valid molecules conditioned on the molecular scaffold and ADMET properties of the input hERG-active molecule, which are filtered based on desired activity against hERG, Nav1.5 and Cav1.2 channels using the discriminative models. The input molecule and each filtered generated molecule are then converted into 209-dimensional chemical descriptor vectors which are refined by removing the redundant descriptors according to pairwise mutual information between every possible descriptor pair. Cosine similarities are then calculated between the descriptor vector of the input molecule and the descriptor vectors of every filtered generated molecule to identify the molecules most chemically similar to the input molecule, but with desired activity against each of the cardiac ion channels.

5.2 Case Study: Optimizing the FDA-Approved Drug Pimozide for Reduced hERG Activity

Pimozide is an FDA-approved antipsychotic agent that is used to treat Tourette's syndrome as well as various other psychiatric disorders.¹⁴⁵ Its main pharmacodynamic action is to blockade dopamine D2 receptors on neurons in the central nervous system; it also has various effects on other central nervous system receptor systems which are not fully characterized.¹²⁸ There are many reports linking the use of pimozide to cardiac action potential prolongation and ventricular arrhythmias,^{146, 147} and there are multiple reported instances of sudden, unexpected deaths of patients receiving pimozide.¹⁴⁸

It was initially observed clinically that only a very low dose of pimozide is necessary to produce QT (Q: start of depolarization; T: end of repolarization) interval prolongation, suggesting that it binds to one or more cardiac potassium ion channels with high affinity.¹⁴⁶ Subsequent experimental validation indicated pimozide's high affinity to the hERG channel, evidenced by its potent inhibitory effect with an IC50 value of approximately 18 nM.¹³¹

Because of pimozide's cardiotoxic effects, it is contraindicated in patients with congenital long QT syndrome, patients with a history of cardiac arrhythmias, patients taking other drugs that prolong the QT interval, and patients with known hypokalemia or hypomagnesemia.¹⁴⁸ It is therefore of tremendous interest to develop safer alternatives to pimozide that retain its therapeutic efficacy while minimizing its hERG channel activity.

In this work, we apply the CardioGenAI framework to re-engineer pimozide for reduced hERG inhibition while preserving its pharmacological activity. The experimentally determined pIC₅₀ of pimozide for the hERG channel is 8.520 and the value that our regression model predicts is 7.629. Our objective is to generate compounds with similar pharmacological properties, but with predicted hERG channel pIC₅₀ values less than 6.0. We therefore condition the molecular generation on the scaffold and ADMET properties of pimozide, and at the generation phase, filter out molecules with a predicted hERG channel pIC₅₀ greater than or equal to 6.0. This procedure is performed until 100 compounds are generated, which takes approximately one minute using an NVIDIA GeForce RTX 4050 GPU. We then compute descriptor vectors for the filtered generated molecules and pimozide, and then calculate the cosine similarities between the descriptor vectors of the generated molecules and that of pimozide.

We calculate the ten ADMET properties for pimozide, the 100 generated molecules, and the molecules in the transformer training set, and then perform principal component analysis (PCA) to construct a lower-dimensional ADMET-based chemical space in which we can compare the generated molecules to pimozide in relation to the broader transformer training set. Plotting the first two PCs reveals that the generated molecules are closely aligned to pimozide, indicating that our framework successfully navigates the initially vast chemical space to propose compounds with similar ADMET characteristics to pimozide while reducing hERG activity (Figure 4; Figure S11 in the *Supporting Information*).

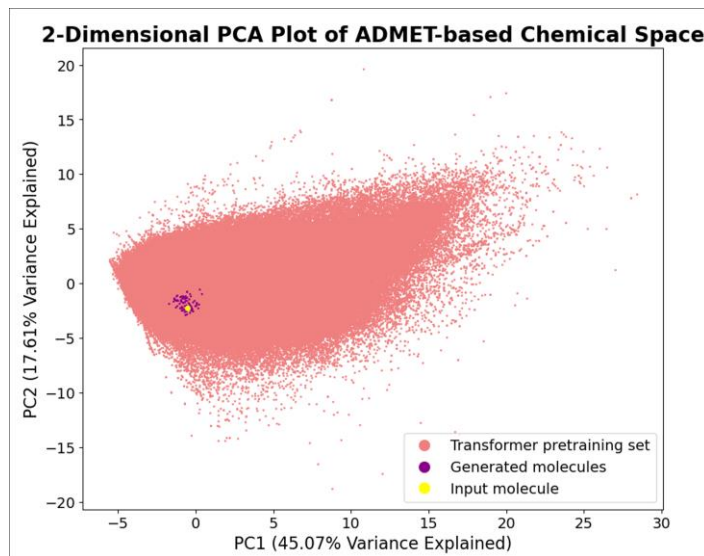


Figure 4. Visualization of the first two principal components of the reduced ADMET-based chemical space. For the input molecule (pimozide), the generated molecules (100 datapoints), and the molecules in the training set for the transformer-based models (approximately 5 million datapoints), ADMET properties are calculated, and principal component analysis is performed to generate a lower-dimensional representation of chemical space. Molecules in the training set of the transformer-based models are colored red, the generated molecules are colored purple, and pimozide is colored yellow. The first two principal components explain 45.07% and 17.61% of the total variance, respectively. Clearly, the generated molecular distribution occupies a precise region within the space that is focused on the input molecule.

Remarkably, among the 100 generated compounds is fluspirilene, a compound that belongs to the same class of drugs (diphenylmethanes) as pimozone and therefore exhibits a highly similar pharmacological profile.¹⁴⁹ Moreover, the predicted hERG channel pIC50 value for fluspirilene is 5.785 (experimental: 5.638), as compared to 7.629 (experimental: 8.520) for pimozone (Figure 5). This case study demonstrates the ability of the CardioGenAI framework to re-engineer a cardiotoxic compound for reduced hERG activity while preserving its pharmacological activity.

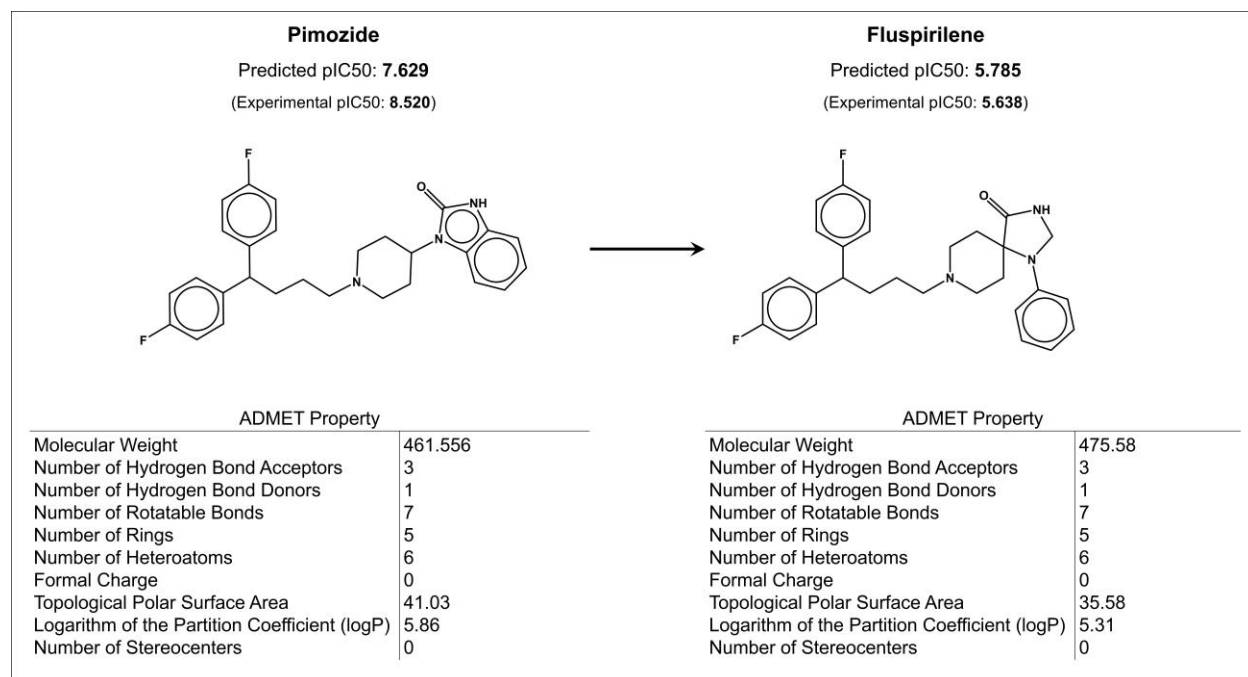


Figure 5. CardioGenAI framework applied to pimozone, an FDA-approved antipsychotic drug that has a predicted hERG channel pIC50 of 7.629, and is reported to cause hERG channel blockade-induced arrhythmias. 100 molecules are generated, and among them is fluspirilene, a compound that belongs to the same class of drugs as pimozone, but exhibits significantly less hERG channel activity (predicted pIC50 value is 5.785).

Additionally, the most similar generated molecules to pimozone as well as an analysis of the predicted pIC50 values of the generated molecules are reported in Table S12 and Figure S13, respectively, of the *Supporting Information*.

6. Summary

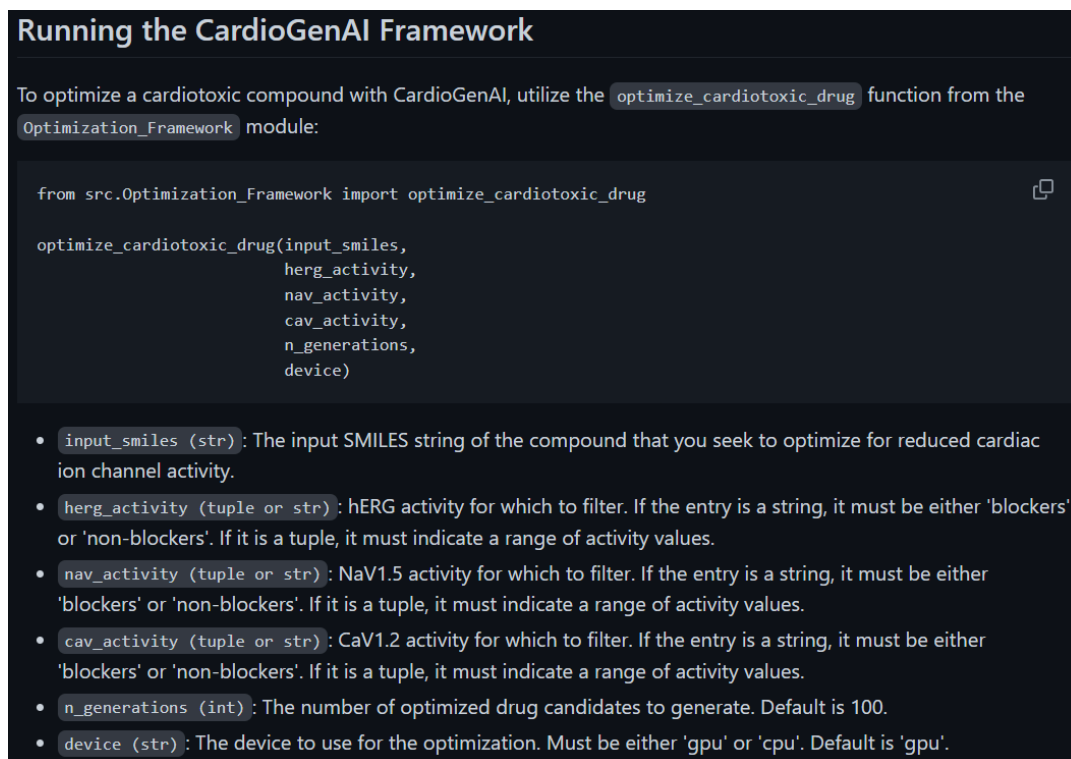
In this work, we present an ML-based framework for re-engineering cardiotoxic compounds for reduced hERG channel activity while preserving their pharmacological activity. The method utilizes an autoregressive transformer-based generative model to produce molecules conditioned on the molecular scaffold and set of ADMET properties of the input molecule. The generated ensemble is filtered based on hERG, Nav1.5 and Cav1.2 activity using discriminative deep learning models. A chemical space representation is then constructed from the filtered generated distribution and the input molecule, where nearby molecules exhibit similar chemical properties,

thus facilitating the identification of molecules with similar pharmacological activity to the input molecule but with reduced hERG liability. We applied the framework to pimoziide, an FDA-approved antipsychotic agent that demonstrates high affinity to the hERG channel, and generate a compound of the same class of drugs that has a significantly lower hERG pIC50.

7. Software Details and Availability

The transformer-based models and the feed-forward networks in the discriminative models are built using PyTorch.¹⁵⁰ The parameters of the transformer-based models are optimized using the Sophia optimizer.¹⁴⁴ The GAT components of the discriminative models are built using PyTorch Geometric.¹⁵¹ The hyperparameters of the discriminative models are optimized using Optuna.¹⁵² SMILES canonicalization, as well as the calculations of ADMET properties and molecular scaffolds were performed using RDKit.¹¹⁰ Scikit-learn was used to calculate pairwise mutual information between chemical features and cosine similarity between descriptor vectors, as well as to perform PCA.¹⁵³

All of our software is available as open source at <https://github.com/gregory-kyro/CardioGenAI>. Users can easily run the complete CardioGenAI framework, perform inference with the discriminative models, and reproduce the figures in this manuscript. We provide all of the data we use, as well as the parameters for each of our trained models.



```
Running the CardioGenAI Framework

To optimize a cardiotoxic compound with CardioGenAI, utilize the optimize_cardiotoxic_drug function from the Optimization_Framework module:

from src.Optimization_Framework import optimize_cardiotoxic_drug

optimize_cardiotoxic_drug(input_smiles,
                          herg_activity,
                          nav_activity,
                          cav_activity,
                          n_generations,
                          device)

• input_smiles (str) : The input SMILES string of the compound that you seek to optimize for reduced cardiac ion channel activity.
• herg_activity (tuple or str) : hERG activity for which to filter. If the entry is a string, it must be either 'blockers' or 'non-blockers'. If it is a tuple, it must indicate a range of activity values.
• nav_activity (tuple or str) : NaV1.5 activity for which to filter. If the entry is a string, it must be either 'blockers' or 'non-blockers'. If it is a tuple, it must indicate a range of activity values.
• cav_activity (tuple or str) : CaV1.2 activity for which to filter. If the entry is a string, it must be either 'blockers' or 'non-blockers'. If it is a tuple, it must indicate a range of activity values.
• n_generations (int) : The number of optimized drug candidates to generate. Default is 100.
• device (str) : The device to use for the optimization. Must be either 'gpu' or 'cpu'. Default is 'gpu'.
```

Figure 6. Python function to run the complete CardioGenAI framework.

Performing Inference with the Discriminative Models

To predict activity against the hERG, Nav1.5 and CaV1.2 channels, utilize the `predict_cardiac_ion_channel_activity` function from the `Discriminator` module:

```
from src.Discriminator import predict_cardiac_ion_channel_activity

predict_cardiac_ion_channel_activity(input_data,
                                    prediction_type,
                                    predict_hERG,
                                    predict_Nav,
                                    predict_Cav,
                                    device)
```

- `input_data (str or list)` : The input data for which the discriminative models will process. If the entry is a string, it must be either a SMILES string or a path to a prepared h5 file. If it is a list, it must be a list of SMILES strings.
- `prediction_type (str)` : Either 'regression' or 'classification'. Default is 'regression'.
- `predict_hERG (bool)` : Whether to predict hERG activity. Default is True.
- `predict_Nav (bool)` : Whether to predict Nav1.5 activity. Default is False.
- `predict_Cav (bool)` : Whether to predict CaV1.2 activity. Default is False.
- `device (str)` : The device to use for the inference computations. Must be either 'gpu' or 'cpu'. Default is 'gpu'.

Figure 7. Python function to perform inference with the discriminative models.

Author Information

Corresponding Authors:

Gregory W. Kyro

- Phone: (516) 413-1143
- Email: gregory.kyro@yale.edu

Victor S. Batista

- Phone: (203) 432-6672
- Email: victor.batista@yale.edu

Present Address: Department of Chemistry, Yale University, New Haven, CT 06511-8499

Author Contributions

GWK conceived the idea; GWK designed research; GWK developed software; GWK performed research; GWK analyzed data; GWK wrote the paper; MTM, EDW, VSB provided feedback on the paper. All authors have given approval to the final version of the manuscript.

Funding Sources

- National Science Foundation Graduate Research Fellowship: Grant DGE-2139841
- National Science Foundation Engines Development Award – Advancing Quantum Technologies (CT): Award Number 2302908
- CCI Phase I – National Science Foundation Center for Quantum Dynamics on Modular Quantum Devices (CQD-MQD): Award Number 2124511
- Yale University: seed funding

Acknowledgments

We acknowledge financial support from the National Science Foundation Graduate Research Fellowship under Grant DGE-2139841 [GWK], from the National Science Foundation Engines Development Award: Advancing Quantum Technologies (CT) under Award Number 2302908 [VSB], and from the CCI Phase I: National Science Foundation Center for Quantum Dynamics on Modular Quantum Devices (CQD-MQD) under Award Number 2124511 [VSB]. Additionally, we acknowledge seed funding from Yale University. We also acknowledge high-performance computer time from the National Energy Research Scientific Computing Center and from the Yale University Faculty of Arts and Sciences High Performance Computing Center.

Abbreviations

ICH, The International Council for Harmonisation of Technical Requirements for Pharmaceuticals for Human Use; $K_v11.1$, voltage-gated potassium ion channel subtype 11.1; hERG, human Ether-à-go-go-Related Gene; CiPA, The Comprehensive In Vitro Proarrhythmia Assay; FDA, U.S. Food and Drug Administration; $Na_v1.5$, voltage-gated sodium ion channel subtype 1.5; $Ca_v1.2$, voltage-gated calcium ion channel subtype 1.2; ML, machine learning; ADMET, absorption, distribution, metabolism, excretion, and toxicity; logP, logarithm of the partition coefficient between n-octanol and water; TPSA, topological polar surface area; ECFP2, Extended-Connectivity Fingerprint with a radius of 2 bonds; GAT, graph attention network; AC, accuracy; SN, sensitivity; SP, specificity; CCR, correct classification rate; MCC, Matthew’s correlation coefficient; AUC, area under the curve; Q , query vector; K , key vector; V , value vector; Q, start of depolarization; T: end of repolarization; PCA, principal component analysis.

Supporting Information

CardioGenAI: A Machine Learning-Based Framework for Re-Engineering Drugs for Reduced hERG Liability

Gregory W. Kyro^{1,*}, Matthew T. Martin², Eric D. Watt², Victor S. Batista^{1,*}

¹Department of Chemistry, Yale University, New Haven, Connecticut 06511

²Drug Safety Research & Development, Pfizer Worldwide Research, Groton, Connecticut 06340

*Correspondence to {gregory.kyro, victor.batista}@yale.edu

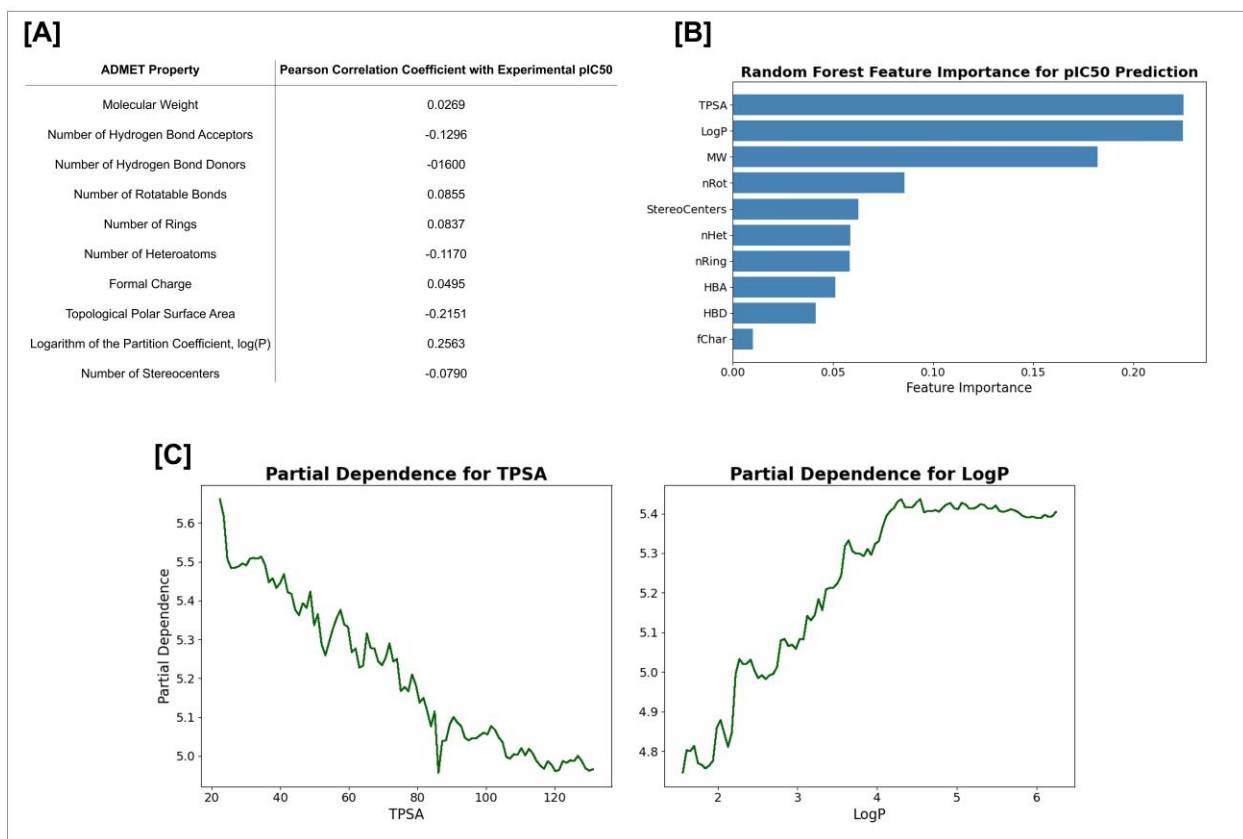


Figure S1. Analysis of the relationships between ADMET properties and experimental hERG channel pIC50 values. In [A], Pearson correlation is shown between each ADMET property and experimental pIC50 values obtained from the training set used. There are noteworthy correlations with pIC50 for topological polar surface area (TPSA) and log(P). A random forest model with 100 estimators was fit to the data to predict pIC50 values, and the importance of each feature was then deduced. In [B], the feature importance of each ADMET property is shown. In [C], the partial dependences for TPSA and log(P) are shown. For log(P), there is an initial positive trend where an increase in log(P) corresponds to an increase in pIC50 values up to a log(P) value of approximately 4. For TPSA, as TPSA increases, pIC50 values generally decrease.

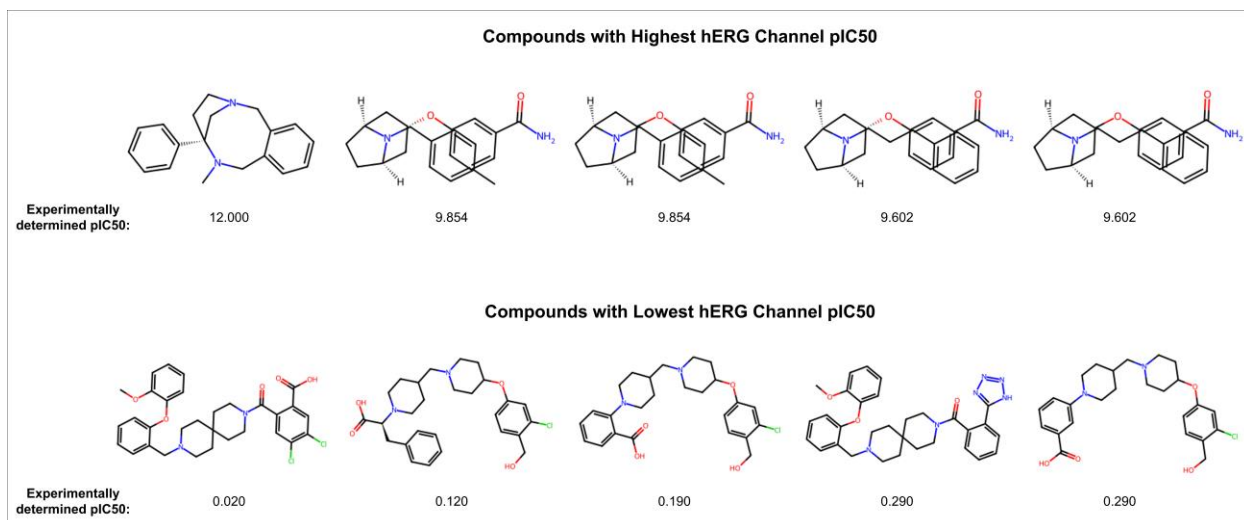


Figure S2. Display of the five compounds with highest hERG channel activity, as well as the five compounds with the lowest hERG channel activity of compounds in the hERG channel training set used. Each molecule is labeled with the corresponding experimentally determined hERG channel pIC50.

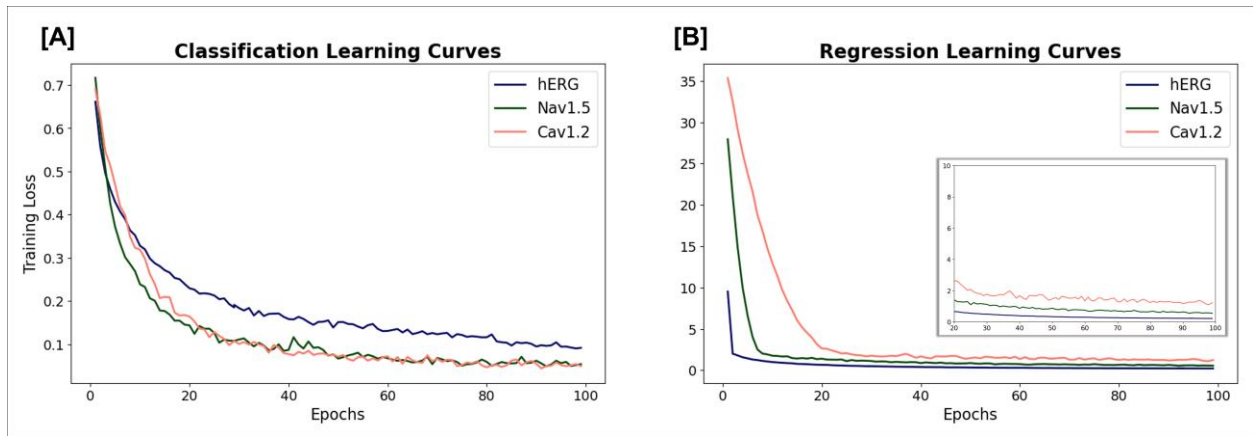


Figure S3. Learning curves for hERG, Nav1.5 and Cav1.2 cardiac ion channel [A] classification and [B] regression models. The classification models are trained with binary cross entropy loss and the AdamW optimizer for 100 epochs. Regression models are trained analogously but using mean squared error loss.

Table S4. Performance regarding each possible feature-representation combination for binary classification of hERG channel blockers.

Feature Representations	AC	SN	SP	F1	CCR	MCC
Transformer feature vector + Graph + Fingerprint	83.5	86.2	80.3	85.1	83.2	66.7
Transformer feature vector + Fingerprint	80.4	82.9	77.3	82.3	80.1	60.4
Transformer feature vector + Graph	80.0	82.9	76.4	81.9	79.6	59.5
Graph + Fingerprint	78.6	80.9	75.9	80.6	78.4	56.8
Transformer feature vector	77.7	83.3	70.9	80.4	77.1	54.9
Fingerprint	76.6	79.3	73.4	78.8	76.3	52.7
Graph	74.4	87.8	58.1	79.0	73.0	48.6

^a The evaluation set used is that developed by Arab et al.; compounds in the evaluation set have a structural similarity (as determined by pairwise Tanimoto similarity between 2048-bit Morgan fingerprints) no greater than 0.70 to any compound in the corresponding training or validation sets.

^b The top value achieved for each metric is shown in bold.

^c Accuracy (AC), sensitivity (SN), specificity (SP), F1-score (F1), correct classification rate (CCR), and Matthew's correlation coefficient (MCC) are shown.

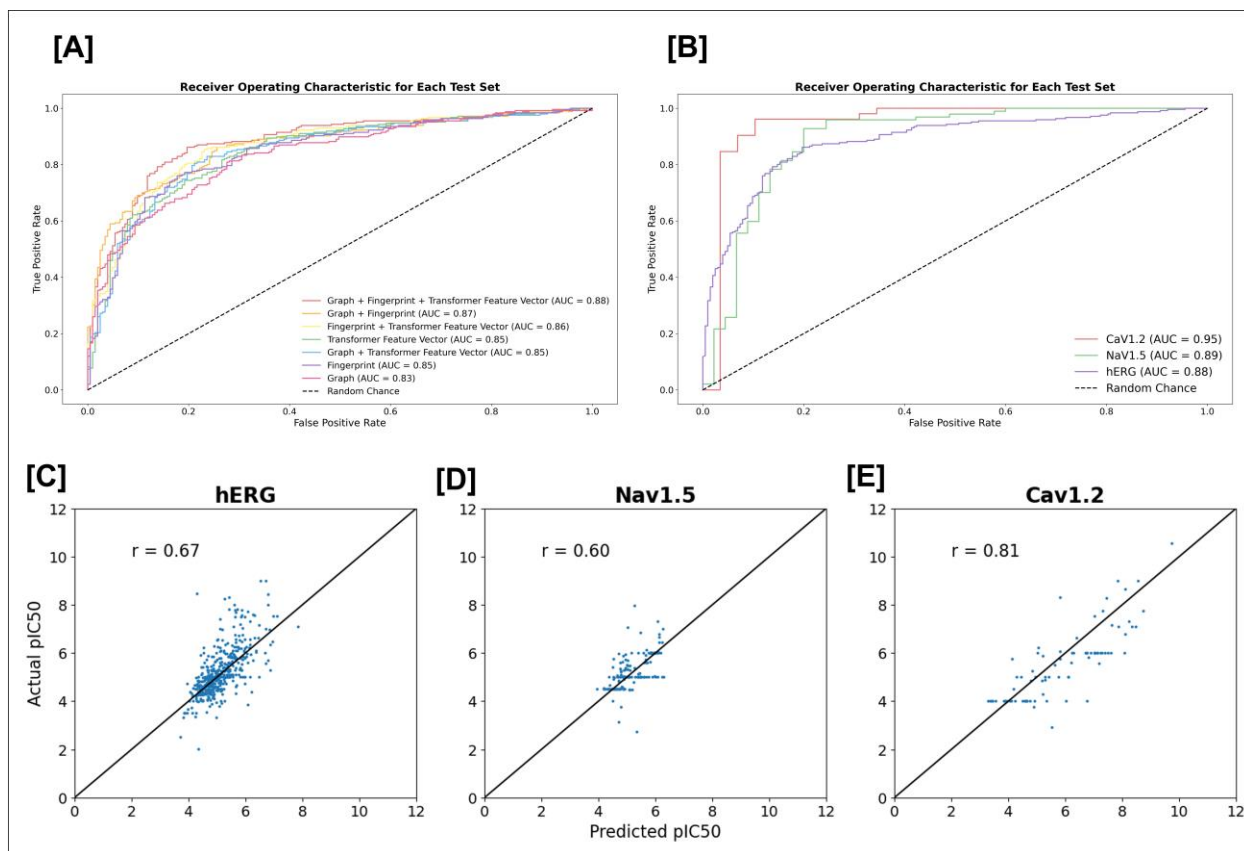


Figure S5. Evaluation of classification and regression models for cardiac ion channel blocker prediction. [A] Receiver operating characteristic (ROC) curve for evaluation on the hERG benchmark presented by Arab et al. Results regarding each feature-representation combination are shown with the corresponding area under the curve (AUC). [B] ROC curve for evaluation on the hERG, Nav_v1.5 and Cav_v1.2 channel benchmarks. Scatter plots depicting actual pIC₅₀ as a function of predicted pIC₅₀, with the corresponding Pearson correlation coefficient (r), shown for evaluation on the [C] hERG, [D] Nav_v1.5, and [E] Cav_v1.2 channel benchmark sets.

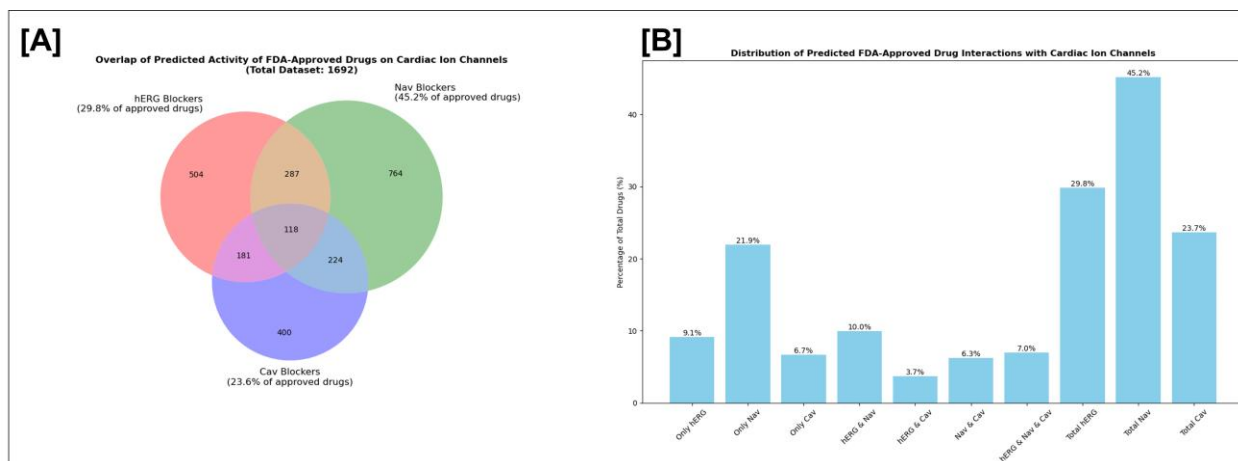


Figure S6. Application of cardiac ion channel classification models to a subset of FDA-approved drugs obtained from DrugCentral. A Venn diagram [A] and bar plot [B] are shown for the screening results of the 1692 total compounds.

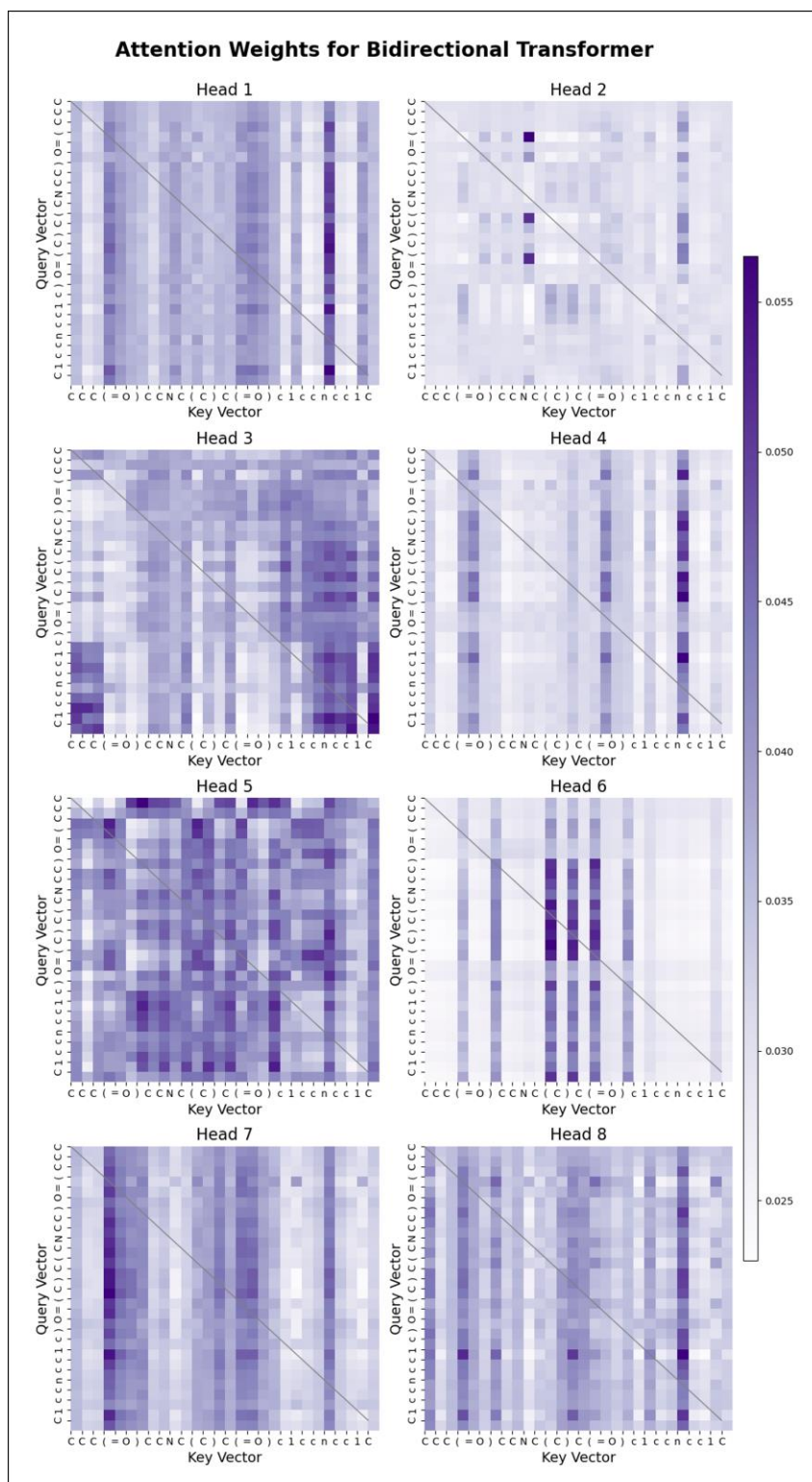


Figure S7. Representative attention maps depicting the distribution of attention weights extracted from the bidirectional transformer trained on SMILES strings, with each subplot corresponding to one of the eight heads in the model's attention layer. Weights are shown for the SMILES string: “CCC(=O)CCNC(C)C(=O)c1ccncc1C”.

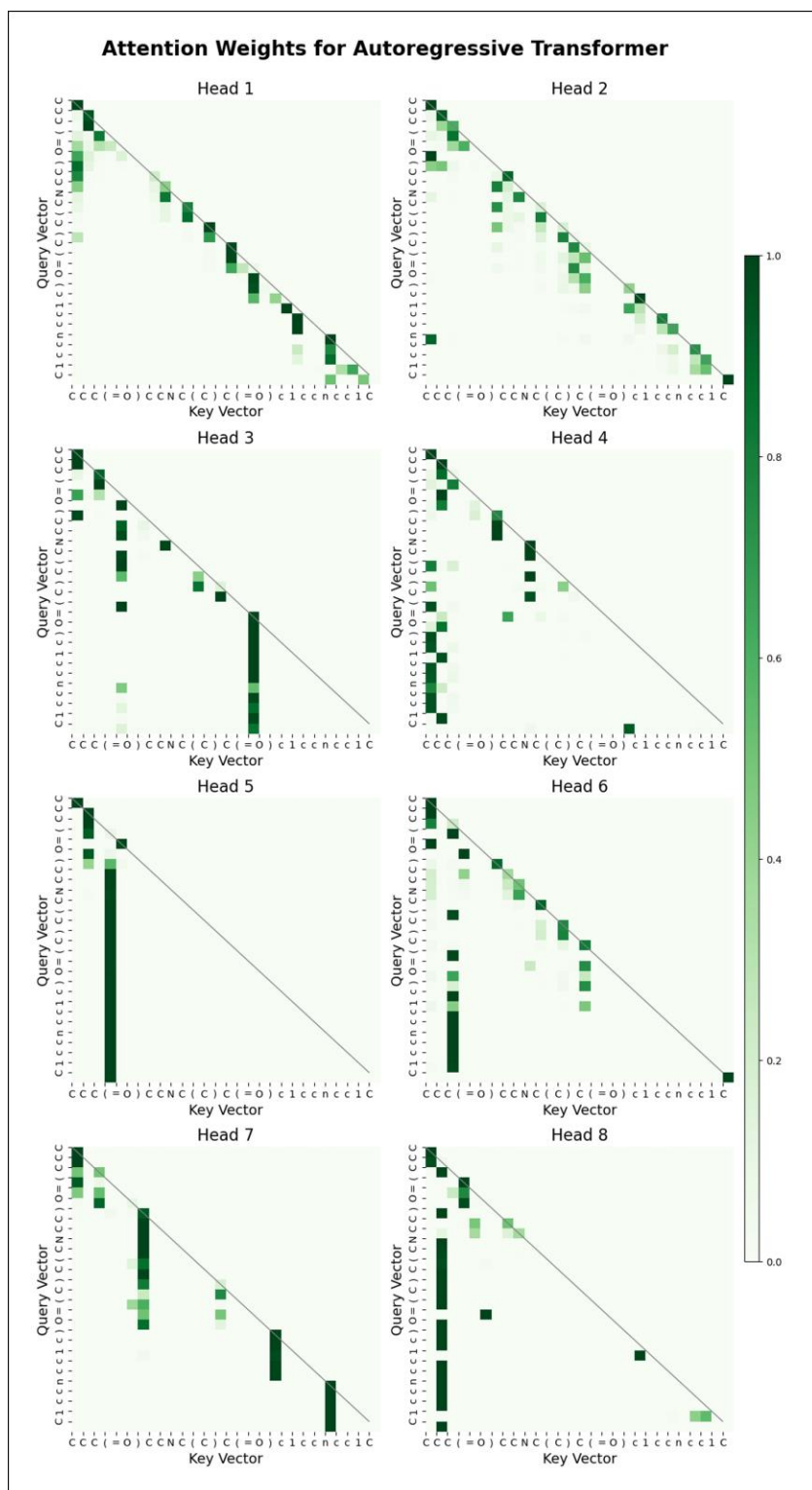


Figure S8. Representative attention maps depicting the distribution of attention weights extracted from the autoregressive transformer trained on SMILES strings, with each subplot corresponding to one of the eight heads in the model's attention layer. Weights are shown for the SMILES string: “CCC(=O)CCNC(C)C(=O)c1ccncc1C”.

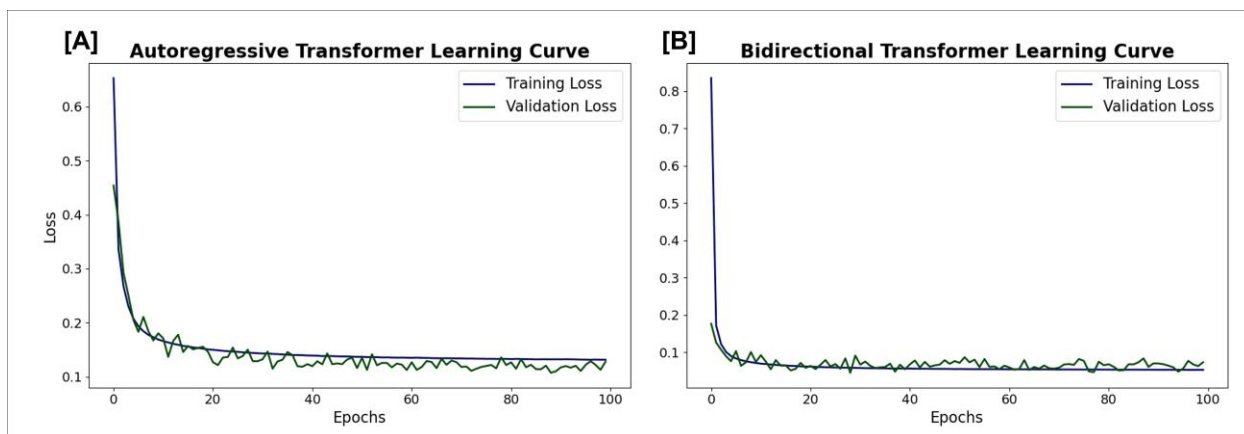


Figure S9. Learning curves for the [A] autoregressive transformer and [B] bidirectional transformer models. The autoregressive transformer is trained for next-token prediction, and the bidirectional transformer is trained for masked-token prediction. Both models are trained with cross entropy loss and the Sophia optimizer for 100 epochs.

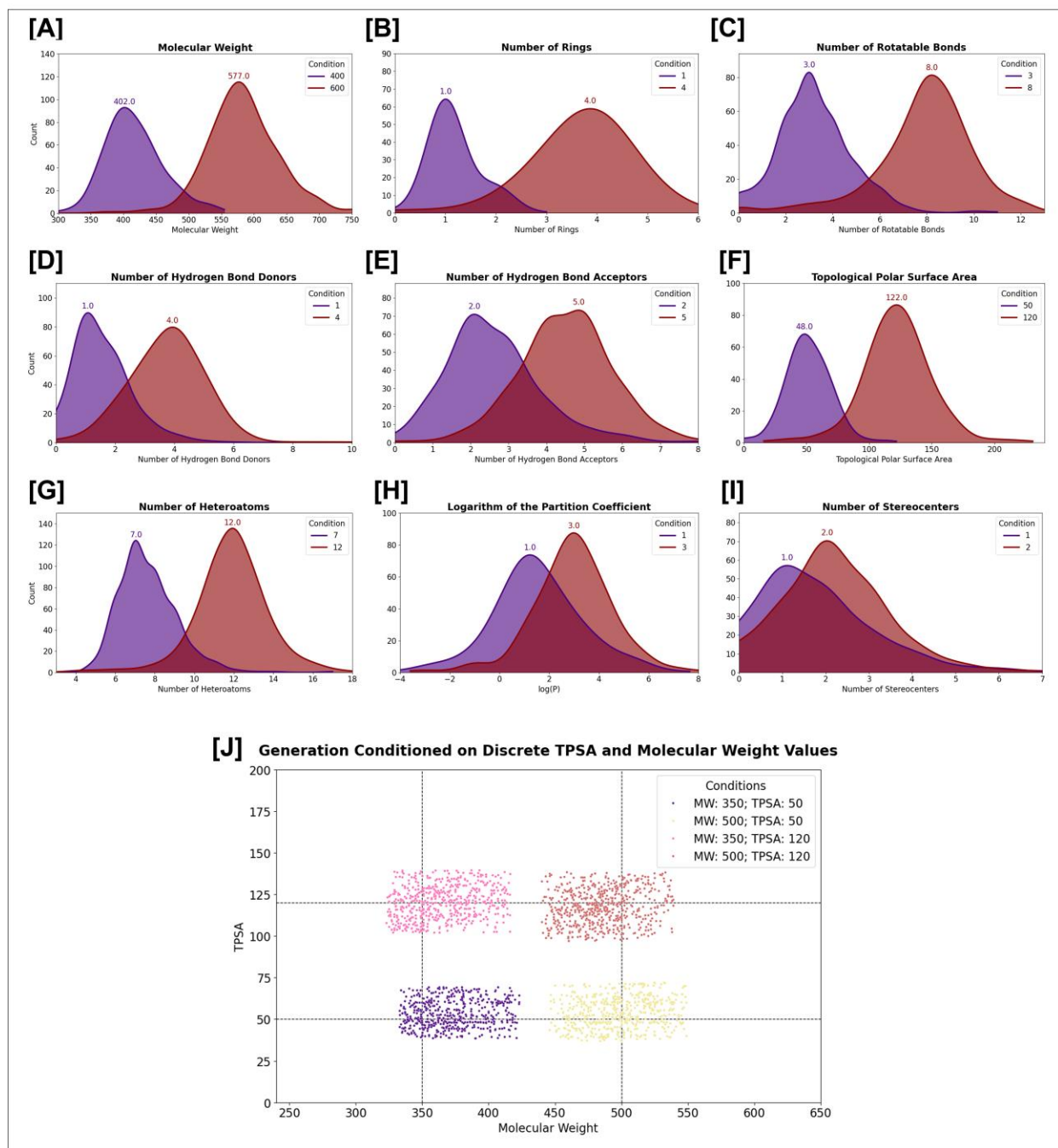


Figure S10. Probing the ability of the generative model to generate distributions of molecules with desired conditions. Results are shown for generations conditioned on different discrete values for [A] molecular weight, [B] number of rings, [C] number of rotatable bonds, [D] number of hydrogen bond donors, [E] number of hydrogen bond acceptors, [F] topological polar surface area, [G] number of heteroatoms, [H] $\log(P)$ (logarithm of the partition coefficient), and [I] number of stereocenters. In [J], the generations are conditioned based on different value combinations of topological polar surface area (TPSA) and molecular weight. For each of the four pairs of conditions, values above/below two standard deviations greater/less than the mean value of each metric are excluded to emphasize the locations of the distribution means.

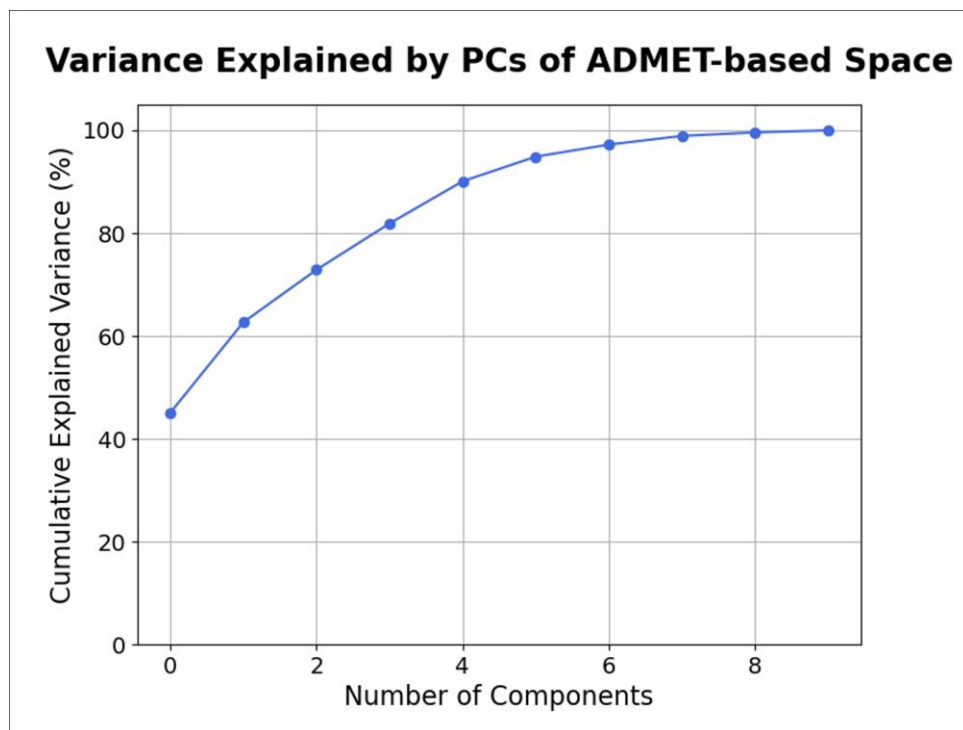


Figure S11. Cumulative variance as a function of principal component for principal component analysis (PCA) of ADMET-based chemical space. For the input cardiotoxic molecule (pimozide), the generated molecules (100 datapoints), and the molecules in the pretraining set for the autoregressive transformer-based generative model (approximately 5 million datapoints), ADMET properties are calculated, and PCA is performed to generate a lower-dimensional representation of chemical space.

Table S12. CardioGenAI methodology applied to pimozide, an FDA-approved antipsychotic drug that has a predicted hERG-channel pIC50 of 7.629, and is reported to cause hERG channel blockade-induced arrhythmias (Table 4). 100 molecules are generated, and among them is fluspirilene, a compound that belongs to the same class of drugs as pimozide and therefore has a similar primary therapeutic mode of action, but exhibits significantly less hERG-channel activity (5.785 pIC50). Included in the table are the five most similar generated compounds to pimozide in terms of cosine similarity between molecular descriptor vectors.

Similarity Rank	SMILES String	Cosine Similarity	Predicted pIC50
Input Molecule	<chem>O=c1[nH]c2ccccc2n1C1CCN(CCCC(c2ccc(F)cc2)c2ccc(F)cc2)CC1</chem> (pimozide)	1.000	7.629
1	<chem>Fc1ccc(CCCN2CCc3c[nH]c(n3)C2)c(N2CCC(c3ccccc3)CC2)c1</chem>	0.980	5.367
2	<chem>O=C(Nc1ccccc1)N(CCCN1CCCC1)CC1(c2ccc(F)cc2)CCC1</chem>	0.977	5.904
3	<chem>O=C(NCc1ccc(F)cc1)N(CCCN1CCCC1)c1cccc2ccccc12</chem>	0.976	5.794
4	<chem>O=C1NCN(c2ccccc2)C12CCN(CCCC(c1ccc(F)cc1)c1ccc(F)cc1)CC2</chem> (fluspirilene)	0.948	5.785
5	<chem>Fc1cccc(Cc2ncc(C3(N4CCC(Cc5ccccc5)CC4)CCOCC3)[nH]2)c1</chem>	0.946	5.201

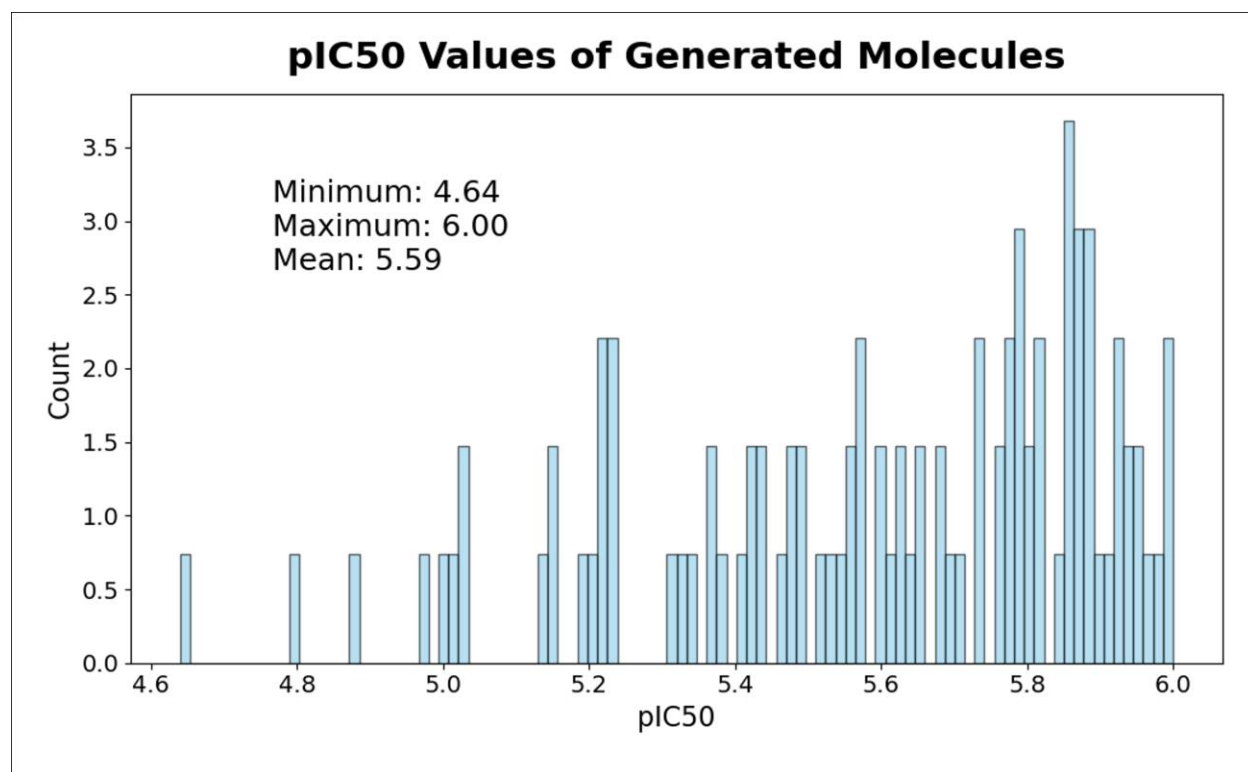


Figure S13. Predicted hERG channel pIC50 values for the 100 generated molecules conditioned on pimozide. The minimum (4.64), mean (5.59) and maximum (6.00) pIC50 values are shown.

References

- (1) Sanguinetti, M. C.; Tristani-Firouzi, M. hERG potassium channels and cardiac arrhythmia. *Nature* **2006**, *440* (7083), 463-469. DOI: 10.1038/nature04710.
- (2) Sun, D.; Gao, W.; Hu, H.; Zhou, S. Why 90% of clinical drug development fails and how to improve it? *Acta Pharmaceutica Sinica B* **2022**, *12* (7), 3049-3062. DOI: <https://doi.org/10.1016/j.apsb.2022.02.002>.
- (3) Group, E. I. W. ICH E14 Guideline: the clinical evaluation of QT/QTc interval prolongation and proarrhythmic potential for non-antiarrhythmic drugs. *Questions & answers (R3)* **2015**.
- (4) Food; Administration, D.; Health, U. D. o.; Services, H. Guidance for industry. E14 clinical evaluation of QT/QTc interval prolongation and proarrhythmic potential for non-antiarrhythmic drugs. <http://www.fda.gov/cder/guidance/6922fnl.pdf> **2005**.
- (5) Jones, D. K.; Liu, F.; Vaidyanathan, R.; Eckhardt, L. L.; Trudeau, M. C.; Robertson, G. A. hERG 1b is critical for human cardiac repolarization. *Proceedings of the National Academy of Sciences* **2014**, *111* (50), 18073-18077. DOI: doi:10.1073/pnas.1414945111.
- (6) Sager, P. T.; Gintant, G.; Turner, J. R.; Pettit, S.; Stockbridge, N. Rechanneling the cardiac proarrhythmia safety paradigm: A meeting report from the Cardiac Safety Research Consortium. *American Heart Journal* **2014**, *167* (3), 292-300. DOI: <https://doi.org/10.1016/j.ahj.2013.11.004>.
- (7) Kowalska, M.; Nowaczyk, J.; Nowaczyk, A. K(V)11.1, Na(V)1.5, and Ca(V)1.2 Transporter Proteins as Antitarget for Drug Cardiotoxicity. *Int J Mol Sci* **2020**, *21* (21). DOI: 10.3390/ijms21218099 From NLM.
- (8) Warner, B.; Hoffmann, P. Investigation of the potential of clozapine to cause torsade de pointes. *Adverse drug reactions and toxicological reviews* **2002**, *21*, 189-203.
- (9) Bril, A.; Gout, B.; Bonhomme, M.; Landais, L.; Faivre, J.-F.; Linee, P.; Poyser, R. H.; Ruffolo, R. Combined potassium and calcium channel blocking activities as a basis for antiarrhythmic efficacy with low proarrhythmic risk: experimental profile of BRL-32872. *Journal of Pharmacology and Experimental Therapeutics* **1996**, *276* (2), 637-646.
- (10) Meyer, T.; Boven, K.-H.; Günther, E.; Fejtl, M. Micro-electrode arrays in cardiac safety pharmacology: a novel tool to study QT interval prolongation. *Drug safety* **2004**, *27*, 763-772.
- (11) Finlayson, K.; Turnbull, L.; January, C. T.; Sharkey, J.; Kelly, J. S. [3H] dofetilide binding to HERG transfected membranes: a potential high throughput preclinical screen. *European journal of pharmacology* **2001**, *430* (1), 147-148.
- (12) Dorn, A.; Hermann, F.; Ebneith, A.; Bothmann, H.; Trube, G.; Christensen, K.; Apfel, C. Evaluation of a high-throughput fluorescence assay method for HERG potassium channel inhibition. *Journal of Biomolecular Screening* **2005**, *10* (4), 339-347.
- (13) Cheng, C. S.; Alderman, D.; Kwash, J.; Dessaint, J.; Patel, R.; Lescoe, M. K.; Kinrade, M. B.; Yu, W. A high-throughput HERG potassium channel function assay: an old assay with a new look. *Drug development and industrial pharmacy* **2002**, *28* (2), 177-191.
- (14) Creanza, T. M.; Delre, P.; Ancona, N.; Lentini, G.; Saviano, M.; Mangiatordi, G. F. Structure-Based Prediction of hERG-Related Cardiotoxicity: A Benchmark Study. *Journal of Chemical Information and Modeling* **2021**, *61* (9), 4758-4770. DOI: 10.1021/acs.jcim.1c00744.
- (15) Kalyanamoorthy, S.; Lamothe, S. M.; Hou, X.; Moon, T. C.; Kurata, H. T.; Houghton, M.; Barakat, K. H. A structure-based computational workflow to predict liability and binding modes of small molecules to hERG. *Scientific Reports* **2020**, *10* (1), 16262. DOI: 10.1038/s41598-020-72889-5.

- (16) Krishna, S.; Borrel, A.; Huang, R.; Zhao, J.; Xia, M.; Kleinstreuer, N. High-Throughput Chemical Screening and Structure-Based Models to Predict hERG Inhibition. *Biology* **2022**, *11* (2), 209.
- (17) Hari Narayana Moorthy, N. S.; Karthikeyan, C.; Manivannan, E. Multi-algorithm based machine learning and structural pattern studies for hERG ion channel blockers mediated cardiotoxicity prediction. *Chemometrics and Intelligent Laboratory Systems* **2021**, *208*, 104213. DOI: <https://doi.org/10.1016/j.chemolab.2020.104213>.
- (18) Ryu, J. Y.; Lee, M. Y.; Lee, J. H.; Lee, B. H.; Oh, K.-S. DeepHIT: a deep learning framework for prediction of hERG-induced cardiotoxicity. *Bioinformatics* **2020**, *36* (10), 3049-3055. DOI: 10.1093/bioinformatics/btaa075 (accessed 2/3/2024).
- (19) Kim, H.; Nam, H. hERG-Att: Self-attention-based deep neural network for predicting hERG blockers. *Computational Biology and Chemistry* **2020**, *87*, 107286. DOI: <https://doi.org/10.1016/j.compbiolchem.2020.107286>.
- (20) Lee, H.-M.; Yu, M.-S.; Kazmi, S. R.; Oh, S. Y.; Rhee, K.-H.; Bae, M.-A.; Lee, B. H.; Shin, D.-S.; Oh, K.-S.; Ceong, H.; et al. Computational determination of hERG-related cardiotoxicity of drug candidates. *BMC Bioinformatics* **2019**, *20* (10), 250. DOI: 10.1186/s12859-019-2814-5.
- (21) Zhang, Y.; Zhao, J.; Wang, Y.; Fan, Y.; Zhu, L.; Yang, Y.; Chen, X.; Lu, T.; Chen, Y.; Liu, H. Prediction of hERG K⁺ channel blockage using deep neural networks. *Chemical Biology & Drug Design* **2019**, *94* (5), 1973-1985. DOI: <https://doi.org/10.1111/cbdd.13600>.
- (22) Choi, K.-E.; Balupuri, A.; Kang, N. S. The Study on the hERG Blocker Prediction Using Chemical Fingerprint Analysis. *Molecules* **2020**, *25* (11), 2615.
- (23) Siramshetty, V. B.; Nguyen, D.-T.; Martinez, N. J.; Southall, N. T.; Simeonov, A.; Zakharov, A. V. Critical Assessment of Artificial Intelligence Methods for Prediction of hERG Channel Inhibition in the “Big Data” Era. *Journal of Chemical Information and Modeling* **2020**, *60* (12), 6007-6019. DOI: 10.1021/acs.jcim.0c00884.
- (24) Meng, J.; Zhang, L.; Wang, L.; Li, S.; Xie, D.; Zhang, Y.; Liu, H. TSSF-hERG: A machine-learning-based hERG potassium channel-specific scoring function for chemical cardiotoxicity prediction. *Toxicology* **2021**, *464*, 153018. DOI: <https://doi.org/10.1016/j.tox.2021.153018>.
- (25) Ogura, K.; Sato, T.; Yuki, H.; Honma, T. Support Vector Machine model for hERG inhibitory activities based on the integrated hERG database using descriptor selection by NSGA-II. *Scientific Reports* **2019**, *9* (1), 12220. DOI: 10.1038/s41598-019-47536-3.
- (26) Liu, M.; Zhang, L.; Li, S.; Yang, T.; Liu, L.; Zhao, J.; Liu, H. Prediction of hERG potassium channel blockage using ensemble learning methods and molecular fingerprints. *Toxicology Letters* **2020**, *332*, 88-96. DOI: <https://doi.org/10.1016/j.toxlet.2020.07.003>.
- (27) Hu, J.; Huang, M.; Ono, N.; Chen-Izu, Y.; Izu, L. T.; Kanaya, S. Cardiotoxicity Prediction Based on Integrated hERG Database with Molecular Convolution Model. In *2019 IEEE International Conference on Bioinformatics and Biomedicine (BIBM)*, 18-21 Nov. 2019, 2019; pp 1500-1503. DOI: 10.1109/BIBM47256.2019.8983163.
- (28) Cai, C.; Guo, P.; Zhou, Y.; Zhou, J.; Wang, Q.; Zhang, F.; Fang, J.; Cheng, F. Deep Learning-Based Prediction of Drug-Induced Cardiotoxicity. *Journal of Chemical Information and Modeling* **2019**, *59* (3), 1073-1084. DOI: 10.1021/acs.jcim.8b00769.
- (29) Wang, T.; Sun, J.; Zhao, Q. Investigating cardiotoxicity related with hERG channel blockers using molecular fingerprints and graph attention mechanism. *Computers in Biology and Medicine* **2023**, *153*, 106464. DOI: <https://doi.org/10.1016/j.compbiomed.2022.106464>.

- (30) Zhang, X.; Mao, J.; Wei, M.; Qi, Y.; Zhang, J. Z. H. HergSPred: Accurate Classification of hERG Blockers/Nonblockers with Machine-Learning Models. *Journal of Chemical Information and Modeling* **2022**, *62* (8), 1830-1839. DOI: 10.1021/acs.jcim.2c00256.
- (31) Kim, H.; Park, M.; Lee, I.; Nam, H. BayeshERG: a robust, reliable and interpretable deep learning model for predicting hERG channel blockers. *Briefings in Bioinformatics* **2022**, *23* (4). DOI: 10.1093/bib/bbac211 (accessed 2/3/2024).
- (32) Karim, A.; Lee, M.; Balle, T.; Sattar, A. CardioTox net: a robust predictor for hERG channel blockade based on deep learning meta-feature ensembles. *Journal of Cheminformatics* **2021**, *13* (1), 60. DOI: 10.1186/s13321-021-00541-z.
- (33) Chen, Y.; Yu, X.; Li, W.; Tang, Y.; Liu, G. In silico prediction of hERG blockers using machine learning and deep learning approaches. *Journal of Applied Toxicology* **2023**, *43* (10), 1462-1475. DOI: <https://doi.org/10.1002/jat.4477>.
- (34) Shan, M.; Jiang, C.; Chen, J.; Qin, L.-P.; Qin, J.-J.; Cheng, G. Predicting hERG channel blockers with directed message passing neural networks. *RSC Advances* **2022**, *12* (6), 3423-3430, 10.1039/D1RA07956E. DOI: 10.1039/D1RA07956E.
- (35) Delre, P.; Lavado, G. J.; Lamanna, G.; Saviano, M.; Roncaglioni, A.; Benfenati, E.; Mangiardi, G. F.; Gadaleta, D. Ligand-based prediction of hERG-mediated cardiotoxicity based on the integration of different machine learning techniques. *Frontiers in Pharmacology* **2022**, *13*, Original Research. DOI: 10.3389/fphar.2022.951083.
- (36) Ding, W.; Nan, Y.; Wu, J.; Han, C.; Xin, X.; Li, S.; Liu, H.; Zhang, L. Combining multi-dimensional molecular fingerprints to predict the hERG cardiotoxicity of compounds. *Computers in Biology and Medicine* **2022**, *144*, 105390. DOI: <https://doi.org/10.1016/j.compbiomed.2022.105390>.
- (37) Konda, L. S. K.; Keerthi Praba, S.; Kristam, R. hERG liability classification models using machine learning techniques. *Computational Toxicology* **2019**, *12*, 100089. DOI: <https://doi.org/10.1016/j.comtox.2019.100089>.
- (38) Feng, H.; Wei, G.-W. Virtual screening of DrugBank database for hERG blockers using topological Laplacian-assisted AI models. *Computers in Biology and Medicine* **2023**, *153*, 106491. DOI: <https://doi.org/10.1016/j.compbiomed.2022.106491>.
- (39) Butler, A.; Helliwell, M. V.; Zhang, Y.; Hancox, J. C.; Dempsey, C. E. An Update on the Structure of hERG. *Frontiers in Pharmacology* **2020**, *10*, Review. DOI: 10.3389/fphar.2019.01572.
- (40) Arab, I.; Egghe, K.; Laukens, K.; Chen, K.; Barakat, K.; Bittremieux, W. Benchmarking of Small Molecule Feature Representations for hERG, Nav1.5, and Cav1.2 Cardiotoxicity Prediction. *Journal of Chemical Information and Modeling* **2023**. DOI: 10.1021/acs.jcim.3c01301.
- (41) Kong, W.; Huang, W.; Peng, C.; Zhang, B.; Duan, G.; Ma, W.; Huang, Z. Multiple machine learning methods aided virtual screening of Nav1.5 inhibitors. *Journal of Cellular and Molecular Medicine* **2023**, *27* (2), 266-276. DOI: <https://doi.org/10.1111/jcmm.17652>.
- (42) Arab, I.; Barakat, K. ToxTree: descriptor-based machine learning models for both hERG and Nav1.5 cardiotoxicity liability predictions. 2021; p arXiv:2112.13467.
- (43) Chen, L.; Jiang, J.; Dou, B.; Feng, H.; Liu, J.; Zhu, Y.; Zhang, B.; Zhou, T.; Wei, G.-W. Machine learning study of the extended drug–target interaction network informed by pain related voltage-gated sodium channels. *PAIN* **9900**, 10.1097/j.pain.0000000000003089. DOI: 10.1097/j.pain.0000000000003089.
- (44) Llanos, M. A.; Enrique, N.; Esteban-López, V.; Scioli-Montoto, S.; Sánchez-Benito, D.; Ruiz, M. E.; Milesi, V.; López, D. E.; Talevi, A.; Martín, P.; Gavernet, L. A Combined Ligand- and

Structure-Based Virtual Screening To Identify Novel NaV1.2 Blockers: In Vitro Patch Clamp Validation and In Vivo Anticonvulsant Activity. *Journal of Chemical Information and Modeling* **2023**, *63* (22), 7083-7096. DOI: 10.1021/acs.jcim.3c00645.

(45) Segler, M. H.; Kogej, T.; Tyrchan, C.; Waller, M. P. Generating focused molecule libraries for drug discovery with recurrent neural networks. *ACS central science* **2018**, *4* (1), 120-131.

(46) Urbina, F.; Lowden, C. T.; Culberson, J. C.; Ekins, S. MegaSyn: integrating generative molecular design, automated analog designer, and synthetic viability prediction. *ACS omega* **2022**, *7* (22), 18699-18713.

(47) Gupta, A.; Müller, A. T.; Huisman, B. J.; Fuchs, J. A.; Schneider, P.; Schneider, G. Generative recurrent networks for de novo drug design. *Molecular informatics* **2018**, *37* (1-2), 1700111.

(48) Xu, M.; Ran, T.; Chen, H. De novo molecule design through the molecular generative model conditioned by 3D information of protein binding sites. *Journal of Chemical Information and Modeling* **2021**, *61* (7), 3240-3254.

(49) Arús-Pous, J.; Blaschke, T.; Ulander, S.; Reymond, J.-L.; Chen, H.; Engkvist, O. Exploring the GDB-13 chemical space using deep generative models. *Journal of cheminformatics* **2019**, *11* (1), 1-14.

(50) Yonchev, D.; Bajorath, J. DeepCOMO: from structure-activity relationship diagnostics to generative molecular design using the compound optimization monitor methodology. *Journal of Computer-Aided Molecular Design* **2020**, *34*, 1207-1218.

(51) Grisoni, F.; Moret, M.; Lingwood, R.; Schneider, G. Bidirectional molecule generation with recurrent neural networks. *Journal of chemical information and modeling* **2020**, *60* (3), 1175-1183.

(52) Zhang, J.; Chen, H. De novo molecule design using molecular generative models constrained by ligand-protein interactions. *Journal of Chemical Information and Modeling* **2022**, *62* (14), 3291-3306.

(53) Arús-Pous, J.; Johansson, S. V.; Prykhodko, O.; Bjerrum, E. J.; Tyrchan, C.; Reymond, J.-L.; Chen, H.; Engkvist, O. Randomized SMILES strings improve the quality of molecular generative models. *Journal of cheminformatics* **2019**, *11* (1), 1-13.

(54) Moret, M.; Friedrich, L.; Grisoni, F.; Merk, D.; Schneider, G. Generative molecular design in low data regimes. *Nature Machine Intelligence* **2020**, *2* (3), 171-180.

(55) Li, X.; Xu, Y.; Yao, H.; Lin, K. Chemical space exploration based on recurrent neural networks: applications in discovering kinase inhibitors. *Journal of cheminformatics* **2020**, *12* (1), 1-13.

(56) Merk, D.; Friedrich, L.; Grisoni, F.; Schneider, G. De novo design of bioactive small molecules by artificial intelligence. *Molecular informatics* **2018**, *37* (1-2), 1700153.

(57) Tan, X.; Jiang, X.; He, Y.; Zhong, F.; Li, X.; Xiong, Z.; Li, Z.; Liu, X.; Cui, C.; Zhao, Q. Automated design and optimization of multitarget schizophrenia drug candidates by deep learning. *European Journal of Medicinal Chemistry* **2020**, *204*, 112572.

(58) Bjerrum, E. J.; Threlfall, R. Molecular generation with recurrent neural networks (RNNs). *arXiv preprint arXiv:1705.04612* **2017**.

(59) Kotsias, P.-C.; Arús-Pous, J.; Chen, H.; Engkvist, O.; Tyrchan, C.; Bjerrum, E. J. Direct steering of de novo molecular generation with descriptor conditional recurrent neural networks. *Nature Machine Intelligence* **2020**, *2* (5), 254-265.

(60) Olivecrona, M.; Blaschke, T.; Engkvist, O.; Chen, H. Molecular de-novo design through deep reinforcement learning. *Journal of cheminformatics* **2017**, *9* (1), 1-14.

(61) Popova, M.; Isayev, O.; Tropsha, A. Deep reinforcement learning for de novo drug design. *Science advances* **2018**, *4* (7), eaap7885.

- (62) Blaschke, T.; Engkvist, O.; Bajorath, J.; Chen, H. Memory-assisted reinforcement learning for diverse molecular de novo design. *Journal of cheminformatics* **2020**, *12* (1), 1-17.
- (63) Yoshimori, A.; Kawasaki, E.; Kanai, C.; Tasaka, T. Strategies for design of molecular structures with a desired pharmacophore using deep reinforcement learning. *Chemical and Pharmaceutical Bulletin* **2020**, *68* (3), 227-233.
- (64) Blaschke, T.; Arús-Pous, J.; Chen, H.; Margreitter, C.; Tyrchan, C.; Engkvist, O.; Papadopoulos, K.; Patronov, A. REINVENT 2.0: an AI tool for de novo drug design. *Journal of chemical information and modeling* **2020**, *60* (12), 5918-5922.
- (65) Korshunova, M.; Huang, N.; Capuzzi, S.; Radchenko, D. S.; Savych, O.; Moroz, Y. S.; Wells, C. I.; Willson, T. M.; Tropsha, A.; Isayev, O. Generative and reinforcement learning approaches for the automated de novo design of bioactive compounds. *Communications Chemistry* **2022**, *5* (1), 129.
- (66) Popova, M.; Shvets, M.; Oliva, J.; Isayev, O. MolecularRNN: Generating realistic molecular graphs with optimized properties. *arXiv preprint arXiv:1905.13372* **2019**.
- (67) Bian, Y.; Wang, J.; Jun, J. J.; Xie, X.-Q. Deep convolutional generative adversarial network (dcGAN) models for screening and design of small molecules targeting cannabinoid receptors. *Molecular pharmaceutics* **2019**, *16* (11), 4451-4460.
- (68) Méndez-Lucio, O.; Baillif, B.; Clevert, D.-A.; Rouquié, D.; Wichard, J. De novo generation of hit-like molecules from gene expression signatures using artificial intelligence. *Nature communications* **2020**, *11* (1), 10.
- (69) De Cao, N.; Kipf, T. MolGAN: An implicit generative model for small molecular graphs. *arXiv preprint arXiv:1805.11973* **2018**.
- (70) Tsujimoto, Y.; Hiwa, S.; Nakamura, Y.; Oe, Y.; Hiroyasu, T. L-MolGAN: An improved implicit generative model for large molecular graphs. **2021**.
- (71) Wang, J.; Chu, Y.; Mao, J.; Jeon, H.-N.; Jin, H.; Zeb, A.; Jang, Y.; Cho, K.-H.; Song, T.; No, K. T. De novo molecular design with deep molecular generative models for PPI inhibitors. *Briefings in Bioinformatics* **2022**, *23* (4). DOI: 10.1093/bib/bbac285 (accessed 2/3/2024).
- (72) Song, T.; Ren, Y.; Wang, S.; Han, P.; Wang, L.; Li, X.; Rodriguez-Patón, A. DNMG: Deep molecular generative model by fusion of 3D information for de novo drug design. *Methods* **2023**, *211*, 10-22. DOI: <https://doi.org/10.1016/j.ymeth.2023.02.001>.
- (73) Bai, Q.; Tan, S.; Xu, T.; Liu, H.; Huang, J.; Yao, X. MolAICal: a soft tool for 3D drug design of protein targets by artificial intelligence and classical algorithm. *Briefings in Bioinformatics* **2020**, *22* (3). DOI: 10.1093/bib/bbaa161 (accessed 2/3/2024).
- (74) Putin, E.; Asadulaev, A.; Ivanenkov, Y.; Aladinskiy, V.; Sanchez-Lengeling, B.; Aspuru-Guzik, A.; Zhavoronkov, A. Reinforced Adversarial Neural Computer for de Novo Molecular Design. *Journal of Chemical Information and Modeling* **2018**, *58* (6), 1194-1204. DOI: 10.1021/acs.jcim.7b00690.
- (75) Lee, Y. J.; Kahng, H.; Kim, S. B. Generative Adversarial Networks for De Novo Molecular Design. *Molecular Informatics* **2021**, *40* (10), 2100045. DOI: <https://doi.org/10.1002/minf.202100045>.
- (76) Putin, E.; Asadulaev, A.; Vanhaelen, Q.; Ivanenkov, Y.; Aladinskaya, A. V.; Aliper, A.; Zhavoronkov, A. Adversarial Threshold Neural Computer for Molecular de Novo Design. *Molecular Pharmaceutics* **2018**, *15* (10), 4386-4397. DOI: 10.1021/acs.molpharmaceut.7b01137.
- (77) Skalic, M.; Sabbadin, D.; Sattarov, B.; Sciabola, S.; De Fabritiis, G. From Target to Drug: Generative Modeling for the Multimodal Structure-Based Ligand Design. *Molecular Pharmaceutics* **2019**, *16* (10), 4282-4291. DOI: 10.1021/acs.molpharmaceut.9b00634.

- (78) Prykhodko, O.; Johansson, S. V.; Kotsias, P.-C.; Arús-Pous, J.; Bjerrum, E. J.; Engkvist, O.; Chen, H. A de novo molecular generation method using latent vector based generative adversarial network. *Journal of Cheminformatics* **2019**, *11* (1), 74. DOI: 10.1186/s13321-019-0397-9.
- (79) Abbasi, M.; Santos, B. P.; Pereira, T. C.; Sofia, R.; Monteiro, N. R. C.; Simões, C. J. V.; Brito, R. M. M.; Ribeiro, B.; Oliveira, J. L.; Arrais, J. P. Designing optimized drug candidates with Generative Adversarial Network. *Journal of Cheminformatics* **2022**, *14* (1), 40. DOI: 10.1186/s13321-022-00623-6.
- (80) Gómez-Bombarelli, R.; Wei, J. N.; Duvenaud, D.; Hernández-Lobato, J. M.; Sánchez-Lengeling, B.; Sheberla, D.; Aguilera-Iparraguirre, J.; Hirzel, T. D.; Adams, R. P.; Aspuru-Guzik, A. Automatic Chemical Design Using a Data-Driven Continuous Representation of Molecules. *ACS Central Science* **2018**, *4* (2), 268-276. DOI: 10.1021/acscentsci.7b00572.
- (81) Lim, J.; Ryu, S.; Kim, J. W.; Kim, W. Y. Molecular generative model based on conditional variational autoencoder for de novo molecular design. *Journal of Cheminformatics* **2018**, *10* (1), 31. DOI: 10.1186/s13321-018-0286-7.
- (82) Wang, S.; Song, T.; Zhang, S.; Jiang, M.; Wei, Z.; Li, Z. Molecular substructure tree generative model for de novo drug design. *Briefings in Bioinformatics* **2022**, *23* (2). DOI: 10.1093/bib/bbab592 (accessed 2/3/2024).
- (83) Kang, S.; Cho, K. Conditional Molecular Design with Deep Generative Models. *Journal of Chemical Information and Modeling* **2019**, *59* (1), 43-52. DOI: 10.1021/acs.jcim.8b00263.
- (84) Lim, J.; Hwang, S.-Y.; Moon, S.; Kim, S.; Kim, W. Y. Scaffold-based molecular design with a graph generative model. *Chemical Science* **2020**, *11* (4), 1153-1164, 10.1039/C9SC04503A. DOI: 10.1039/C9SC04503A.
- (85) Dollar, O.; Joshi, N.; Beck, D. A. C.; Pfendtner, J. Attention-based generative models for de novo molecular design. *Chemical Science* **2021**, *12* (24), 8362-8372, 10.1039/D1SC01050F. DOI: 10.1039/D1SC01050F.
- (86) Krishnan, S. R.; Bung, N.; Vangala, S. R.; Srinivasan, R.; Bulusu, G.; Roy, A. De Novo Structure-Based Drug Design Using Deep Learning. *Journal of Chemical Information and Modeling* **2022**, *62* (21), 5100-5109. DOI: 10.1021/acs.jcim.1c01319.
- (87) Zhavoronkov, A.; Ivanenkov, Y. A.; Aliper, A.; Veselov, M. S.; Aladinskiy, V. A.; Aladinskaya, A. V.; Terentiev, V. A.; Polykovskiy, D. A.; Kuznetsov, M. D.; Asadulaev, A.; et al. Deep learning enables rapid identification of potent DDR1 kinase inhibitors. *Nature Biotechnology* **2019**, *37* (9), 1038-1040. DOI: 10.1038/s41587-019-0224-x.
- (88) Nesterov, V. I.; Wieser, M.; Roth, V. 3DMolNet: A Generative Network for Molecular Structures. *ArXiv* **2020**, *abs/2010.06477*.
- (89) Skalic, M.; Jiménez, J.; Sabbadin, D.; De Fabritiis, G. Shape-Based Generative Modeling for de Novo Drug Design. *Journal of Chemical Information and Modeling* **2019**, *59* (3), 1205-1214. DOI: 10.1021/acs.jcim.8b00706.
- (90) Hong, S. H.; Ryu, S.; Lim, J.; Kim, W. Y. Molecular Generative Model Based on an Adversarially Regularized Autoencoder. *Journal of Chemical Information and Modeling* **2020**, *60* (1), 29-36. DOI: 10.1021/acs.jcim.9b00694.
- (91) Kadurin, A.; Aliper, A.; Kazennov, A.; Mamoshina, P.; Vanhaelen, Q.; Khrabrov, K.; Zhavoronkov, A. The cornucopia of meaningful leads: Applying deep adversarial autoencoders for new molecule development in oncology. *Oncotarget* **2017**, *8* (7), 10883-10890. DOI: 10.18632/oncotarget.14073 From NLM.
- (92) Kadurin, A.; Nikolenko, S.; Khrabrov, K.; Aliper, A.; Zhavoronkov, A. druGAN: An Advanced Generative Adversarial Autoencoder Model for de Novo Generation of New Molecules

- with Desired Molecular Properties in Silico. *Molecular Pharmaceutics* **2017**, *14* (9), 3098-3104. DOI: 10.1021/acs.molpharmaceut.7b00346.
- (93) Polykovskiy, D.; Zhebrak, A.; Vetrov, D.; Ivanenkov, Y.; Aladinskiy, V.; Mamoshina, P.; Bozdaganyan, M.; Aliper, A.; Zhavoronkov, A.; Kadurin, A. Entangled Conditional Adversarial Autoencoder for de Novo Drug Discovery. *Molecular Pharmaceutics* **2018**, *15* (10), 4398-4405. DOI: 10.1021/acs.molpharmaceut.8b00839.
- (94) Winter, R.; Montanari, F.; Steffen, A.; Briem, H.; Noé, F.; Clevert, D.-A. Efficient multi-objective molecular optimization in a continuous latent space. *Chemical Science* **2019**, *10* (34), 8016-8024, 10.1039/C9SC01928F. DOI: 10.1039/C9SC01928F.
- (95) Gao, K.; Nguyen, D. D.; Tu, M.; Wei, G.-W. Generative Network Complex for the Automated Generation of Drug-like Molecules. *Journal of Chemical Information and Modeling* **2020**, *60* (12), 5682-5698. DOI: 10.1021/acs.jcim.0c00599.
- (96) Sattarov, B.; Baskin, I. I.; Horvath, D.; Marcou, G.; Bjerrum, E. J.; Varnek, A. De Novo Molecular Design by Combining Deep Autoencoder Recurrent Neural Networks with Generative Topographic Mapping. *Journal of Chemical Information and Modeling* **2019**, *59* (3), 1182-1196. DOI: 10.1021/acs.jcim.8b00751.
- (97) Mao, J.; Wang, J.; Zeb, A.; Cho, K.-H.; Jin, H.; Kim, J.; Lee, O.; Wang, Y.; No, K. T. Transformer-Based Molecular Generative Model for Antiviral Drug Design. *Journal of Chemical Information and Modeling* **2023**. DOI: 10.1021/acs.jcim.3c00536.
- (98) Wei, L.; Fu, N.; Song, Y.; Wang, Q.; Hu, J. Probabilistic generative transformer language models for generative design of molecules. *Journal of Cheminformatics* **2023**, *15* (1), 88. DOI: 10.1186/s13321-023-00759-z.
- (99) Wang, J.; Mao, J.; Wang, M.; Le, X.; Wang, Y. Explore drug-like space with deep generative models. *Methods* **2023**, *210*, 52-59. DOI: <https://doi.org/10.1016/j.ymeth.2023.01.004>.
- (100) Grechishnikova, D. Transformer neural network for protein-specific de novo drug generation as a machine translation problem. *Scientific Reports* **2021**, *11* (1), 321. DOI: 10.1038/s41598-020-79682-4.
- (101) Kim, H.; Na, J.; Lee, W. B. Generative Chemical Transformer: Neural Machine Learning of Molecular Geometric Structures from Chemical Language via Attention. *Journal of Chemical Information and Modeling* **2021**, *61* (12), 5804-5814. DOI: 10.1021/acs.jcim.1c01289.
- (102) Wang, W.; Wang, Y.; Zhao, H.; Sciabola, S. A Transformer-based Generative Model for De Novo Molecular Design. 2022; p arXiv:2210.08749.
- (103) Chen, Y.; Wang, Z.; Wang, L.; Wang, J.; Li, P.; Cao, D.; Zeng, X.; Ye, X.; Sakurai, T. Deep generative model for drug design from protein target sequence. *Journal of Cheminformatics* **2023**, *15* (1), 38. DOI: 10.1186/s13321-023-00702-2.
- (104) Bagal, V.; Aggarwal, R.; Vinod, P. K.; Priyakumar, U. D. MolGPT: Molecular Generation Using a Transformer-Decoder Model. *Journal of Chemical Information and Modeling* **2022**, *62* (9), 2064-2076. DOI: 10.1021/acs.jcim.1c00600.
- (105) Kyro, G. W.; Morgunov, A.; Brent, R. I.; Batista, V. S. ChemSpaceAL: An Efficient Active Learning Methodology Applied to Protein-Specific Molecular Generation. *Journal of Chemical Information and Modeling* **2024**. DOI: 10.1021/acs.jcim.3c01456.
- (106) Mendez, D.; Gaulton, A.; Bento, A. P.; Chambers, J.; De Veij, M.; Félix, E.; Magariños, M. P.; Mosquera, J. F.; Mutowo, P.; Nowotka, M. ChEMBL: towards direct deposition of bioassay data. *Nucleic acids research* **2019**, *47* (D1), D930-D940.
- (107) Brown, N.; Fiscato, M.; Segler, M. H.; Vaucher, A. C. GuacaMol: benchmarking models for de novo molecular design. *Journal of chemical information and modeling* **2019**, *59* (3), 1096-1108.

- (108) Polykovskiy, D.; Zhebrak, A.; Sanchez-Lengeling, B.; Golovanov, S.; Tatanov, O.; Belyaev, S.; Kurbanov, R.; Artamonov, A.; Aladinskiy, V.; Veselov, M. Molecular sets (MOSES): a benchmarking platform for molecular generation models. *Frontiers in pharmacology* **2020**, *11*, 565644.
- (109) Liu, T.; Lin, Y.; Wen, X.; Jorissen, R. N.; Gilson, M. K. BindingDB: a web-accessible database of experimentally determined protein–ligand binding affinities. *Nucleic Acids Research* **2006**, *35* (suppl_1), D198-D201. DOI: 10.1093/nar/gkl999 (accessed 2/4/2024).
- (110) Landrum, G. Rdkit: Open-source cheminformatics software. **2016**.
- (111) Liu, L.-l.; Lu, J.; Lu, Y.; Zheng, M.-y.; Luo, X.-m.; Zhu, W.-l.; Jiang, H.-l.; Chen, K.-x. Novel Bayesian classification models for predicting compounds blocking hERG potassium channels. *Acta Pharmacologica Sinica* **2014**, *35* (8), 1093-1102. DOI: 10.1038/aps.2014.35.
- (112) Gaulton, A.; Bellis, L. J.; Bento, A. P.; Chambers, J.; Davies, M.; Hersey, A.; Light, Y.; McGlinchey, S.; Michalovich, D.; Al-Lazikani, B.; Overington, J. P. ChEMBL: a large-scale bioactivity database for drug discovery. *Nucleic Acids Research* **2011**, *40* (D1), D1100-D1107. DOI: 10.1093/nar/gkr777 (accessed 2/4/2024).
- (113) Bento, A. P.; Gaulton, A.; Hersey, A.; Bellis, L. J.; Chambers, J.; Davies, M.; Krüger, F. A.; Light, Y.; Mak, L.; McGlinchey, S.; et al. The ChEMBL bioactivity database: an update. *Nucleic Acids Research* **2013**, *42* (D1), D1083-D1090. DOI: 10.1093/nar/gkt1031 (accessed 2/4/2024).
- (114) Gaulton, A.; Hersey, A.; Nowotka, M.; Bento, A. P.; Chambers, J.; Mendez, D.; Mutowo, P.; Atkinson, F.; Bellis, L. J.; Cibrián-Uhalte, E.; et al. The ChEMBL database in 2017. *Nucleic Acids Research* **2016**, *45* (D1), D945-D954. DOI: 10.1093/nar/gkw1074 (accessed 2/4/2024).
- (115) Kim, S.; Chen, J.; Cheng, T.; Gindulyte, A.; He, J.; He, S.; Li, Q.; Shoemaker, B. A.; Thiessen, P. A.; Yu, B.; et al. PubChem in 2021: new data content and improved web interfaces. *Nucleic Acids Research* **2020**, *49* (D1), D1388-D1395. DOI: 10.1093/nar/gkaa971 (accessed 2/4/2024).
- (116) Gilson, M. K.; Liu, T.; Baitaluk, M.; Nicola, G.; Hwang, L.; Chong, J. BindingDB in 2015: A public database for medicinal chemistry, computational chemistry and systems pharmacology. *Nucleic Acids Research* **2015**, *44* (D1), D1045-D1053. DOI: 10.1093/nar/gkv1072 (accessed 2/4/2024).
- (117) hERGCentral: A Large Database to Store, Retrieve, and Analyze Compound-Human Ether-à-go-go Related Gene Channel Interactions to Facilitate Cardiotoxicity Assessment in Drug Development. *ASSAY and Drug Development Technologies* **2011**, *9* (6), 580-588. DOI: 10.1089/adt.2011.0425.
- (118) Didziapetris, R.; Lanevskij, K. Compilation and physicochemical classification analysis of a diverse hERG inhibition database. *Journal of Computer-Aided Molecular Design* **2016**, *30* (12), 1175-1188. DOI: 10.1007/s10822-016-9986-0.
- (119) Doddareddy, M. R.; Klaasse, E. C.; Shagufta; IJzerman, A. P.; Bender, A. Prospective Validation of a Comprehensive In silico hERG Model and its Applications to Commercial Compound and Drug Databases. *ChemMedChem* **2010**, *5* (5), 716-729. DOI: <https://doi.org/10.1002/cmdc.201000024>.
- (120) Munawar, S.; Vandenberg, J. I.; Jabeen, I. Molecular Docking Guided Grid-Independent Descriptor Analysis to Probe the Impact of Water Molecules on Conformational Changes of hERG Inhibitors in Drug Trapping Phenomenon. *International Journal of Molecular Sciences* **2019**, *20* (14), 3385.
- (121) Xiong, G.; Wu, Z.; Yi, J.; Fu, L.; Yang, Z.; Hsieh, C.; Yin, M.; Zeng, X.; Wu, C.; Lu, A.; et al. ADMETlab 2.0: an integrated online platform for accurate and comprehensive predictions of

ADMET properties. *Nucleic Acids Research* **2021**, *49* (W1), W5-W14. DOI: 10.1093/nar/gkab255 (accessed 2/6/2024).

(122) Yang, H.; Lou, C.; Sun, L.; Li, J.; Cai, Y.; Wang, Z.; Li, W.; Liu, G.; Tang, Y. admetSAR 2.0: web-service for prediction and optimization of chemical ADMET properties. *Bioinformatics* **2018**, *35* (6), 1067-1069. DOI: 10.1093/bioinformatics/bty707 (accessed 2/15/2024).

(123) Avram, S.; Bologna, C. G.; Holmes, J.; Bocci, G.; Wilson, T. B.; Nguyen, D. T.; Curpan, R.; Halip, L.; Bora, A.; Yang, J. J.; et al. DrugCentral 2021 supports drug discovery and repositioning. *Nucleic Acids Res* **2021**, *49* (D1), D1160-d1169. DOI: 10.1093/nar/gkaa997 From NLM.

(124) Ursu, O.; Holmes, J.; Knockel, J.; Bologna, C. G.; Yang, J. J.; Mathias, S. L.; Nelson, S. J.; Oprea, T. I. DrugCentral: online drug compendium. *Nucleic Acids Research* **2016**, *45* (D1), D932-D939. DOI: 10.1093/nar/gkw993 (accessed 2/5/2024).

(125) Murray, K. T. Ibutilide. *Circulation* **1998**, *97* (5), 493-497.

(126) Mounsey, J. P.; DiMarco, J. P. Dofetilide. *Circulation* **2000**, *102* (21), 2665-2670.

(127) Mason, J. W. Amiodarone. *New England Journal of Medicine* **1987**, *316* (8), 455-466.

(128) FINDER, R.; BROGDEN, R.; SAWYER, P. R.; SPEIGHT, T.; SPENCER, R.; AVERY, G. Pimozide: a review of its pharmacological properties and therapeutic uses in psychiatry. *Drugs* **1976**, *12*, 1-40.

(129) Henzi, I.; Sonderegger, J.; Tramer, M. R. Efficacy, dose-response, and adverse effects of droperidol for prevention of postoperative nausea and vomiting. *Canadian Journal of Anesthesia* **2000**, *47*, 537-551.

(130) Beresford, R.; Ward, A. Haloperidol decanoate: a preliminary review of its pharmacodynamic and pharmacokinetic properties and therapeutic use in psychosis. *Drugs* **1987**, *33*, 31-49.

(131) Kang, J.; Wang, L.; Cai, F.; Rampe, D. High affinity blockade of the HERG cardiac K⁺ channel by the neuroleptic pimozide. *European Journal of Pharmacology* **2000**, *392* (3), 137-140. DOI: [https://doi.org/10.1016/S0014-2999\(00\)00123-0](https://doi.org/10.1016/S0014-2999(00)00123-0).

(132) DROLET, B.; ZHANG, S.; DESCHÊNES, D.; RAIL, J.; NADEAU, S.; ZHOU, Z.; JANUARY, C. T.; TURGEON, J. Droperidol Lengthens Cardiac Repolarization due to Block of the Rapid Component of the Delayed Rectifier Potassium Current. *Journal of Cardiovascular Electrophysiology* **1999**, *10* (12), 1597-1604. DOI: <https://doi.org/10.1111/j.1540-8167.1999.tb00224.x>.

(133) Lin, Y.; Sun, I.-W.; Liu, S.-I.; Chen, C.-Y.; Hsu, C.-C. QTc prolongation during concurrent treatment with depot antipsychotics and high-dose amisulpride: a report of 2 cases. *J Intern Med Taiwan* **2009**, *20* (6), 544-549.

(134) Richards, D.; Brogden, R.; Heel, R.; Speight, T.; Avery, G. Astemizole: a review of its pharmacodynamic properties and therapeutic efficacy. *Drugs* **1984**, *28*, 38-61.

(135) Badwan, A. A.; Al Kaysi, H. N.; Owais, L. B.; Salem, M. S.; Arafat, T. A. Terfenadine. In *Analytical Profiles of Drug Substances*, Vol. 19; Elsevier, 1990; pp 627-662.

(136) ZHOU, Z.; VORPERIAN, V. R.; GONG, Q.; ZHANG, S.; JANUARY, C. T. Block of HERG Potassium Channels by the Antihistamine Astemizole and its Metabolites Desmethylastemizole and Norastemizole. *Journal of Cardiovascular Electrophysiology* **1999**, *10* (6), 836-843. DOI: <https://doi.org/10.1111/j.1540-8167.1999.tb00264.x>.

(137) Suessbrich, H.; Waldegger, S.; Lang, F.; Busch, A. Blockade of HERG channels expressed in *Xenopus* oocytes by the histamine receptor antagonists terfenadine and astemizole. *FEBS letters* **1996**, *385* (1-2), 77-80.

(138) Huang, Z.; Li, H.; Zhang, Q.; Lu, F.; Hong, M.; Zhang, Z.; Guo, X.; Zhu, Y.; Li, S.; Liu, H. Discovery of Indolinone-Based Multikinase Inhibitors as Potential Therapeutics for Idiopathic

- Pulmonary Fibrosis. *ACS Medicinal Chemistry Letters* **2017**, *8* (11), 1142-1147. DOI: 10.1021/acsmchemlett.7b00164.
- (139) Traebert, M.; Dumotier, B.; Meister, L.; Hoffmann, P.; Dominguez-Estevez, M.; Suter, W. Inhibition of hERG K⁺ currents by antimalarial drugs in stably transfected HEK293 cells. *European Journal of Pharmacology* **2004**, *484* (1), 41-48. DOI: <https://doi.org/10.1016/j.ejphar.2003.11.003>.
- (140) Wang, N.; Yang, Y.; Wen, J.; Fan, X.-R.; Li, J.; Xiong, B.; Zhang, J.; Zeng, B.; Shen, J.-W.; Chen, G.-L. Molecular Determinants for the High-Affinity Blockade of Human Ether-à-go-go-Related Gene K⁺ Channel by Tolterodine. *Journal of Cardiovascular Pharmacology* **2022**, *80* (5), 679-689. DOI: 10.1097/fjc.0000000000001336.
- (141) Wishart, D. S.; Knox, C.; Guo, A. C.; Shrivastava, S.; Hassanali, M.; Stothard, P.; Chang, Z.; Woolsey, J. DrugBank: a comprehensive resource for in silico drug discovery and exploration. *Nucleic Acids Res* **2006**, *34* (Database issue), D668-672. DOI: 10.1093/nar/gkj067 From NLM.
- (142) Wishart, D. S.; Knox, C.; Guo, A. C.; Cheng, D.; Shrivastava, S.; Tzur, D.; Gautam, B.; Hassanali, M. DrugBank: a knowledgebase for drugs, drug actions and drug targets. *Nucleic Acids Res* **2008**, *36* (Database issue), D901-906. DOI: 10.1093/nar/gkm958 From NLM.
- (143) Bemis, G. W.; Murcko, M. A. The properties of known drugs. 1. Molecular frameworks. *J Med Chem* **1996**, *39* (15), 2887-2893. DOI: 10.1021/jm9602928 From NLM.
- (144) Liu, H.; Li, Z.; Hall, D.; Liang, P.; Ma, T. Sophia: A Scalable Stochastic Second-order Optimizer for Language Model Pre-training. 2023; p arXiv:2305.14342.
- (145) Opler, L. A.; Feinberg, S. S. The role of pimozide in clinical psychiatry: a review. *The Journal of clinical psychiatry* **1991**, *52* (5), 221-233.
- (146) Fulop, G.; Phillips, R.; Shapiro, A.; Gomes, J.; Shapiro, E.; Nordlie, J. ECG changes during haloperidol and pimozide treatment of Tourette's disorder. *The American journal of psychiatry* **1987**, *144* (5), 673-675.
- (147) Krähenbühl, S.; Sauter, B.; Kupferschmidt, H.; Krause, M.; Wyss, P. A.; Meier, P. J. Reversible QT prolongation with torsades de pointes in a patient with pimozide intoxication. *The American journal of the medical sciences* **1995**, *309* (6), 315-316.
- (148) Food; Administration, D.; Health, U. D. o.; Services, H. ORAP® (Pimozide) Tablets https://www.accessdata.fda.gov/drugsatfda_docs/label/2009/017473s041lbl.pdf **2008**.
- (149) Qar, J.; Galizzi, J.-P.; Fosset, M.; Lazdunski, M. Receptors for diphenylbutylpiperidine neuroleptics in brain, cardiac, and smooth muscle membranes. Relationship with receptors for 1,4-dihydropyridines and phenylalkylamines and with Ca²⁺ channel blockade. *European Journal of Pharmacology* **1987**, *141* (2), 261-268. DOI: [https://doi.org/10.1016/0014-2999\(87\)90271-8](https://doi.org/10.1016/0014-2999(87)90271-8).
- (150) Paszke, A.; Gross, S.; Massa, F.; Lerer, A.; Bradbury, J.; Chanan, G.; Killeen, T.; Lin, Z.; Gimelshein, N.; Antiga, L.; et al. PyTorch: An Imperative Style, High-Performance Deep Learning Library. 2019; p arXiv:1912.01703.
- (151) Fey, M.; Lenssen, J. E. Fast Graph Representation Learning with PyTorch Geometric. 2019; p arXiv:1903.02428.
- (152) Akiba, T.; Sano, S.; Yanase, T.; Ohta, T.; Koyama, M. Optuna: A Next-generation Hyperparameter Optimization Framework. 2019; p arXiv:1907.10902.
- (153) Pedregosa, F.; Varoquaux, G.; Gramfort, A.; Michel, V.; Thirion, B.; Grisel, O.; Blondel, M.; Müller, A.; Nothman, J.; Louppe, G.; et al. Scikit-learn: Machine Learning in Python. *Journal of Machine Learning Research* **2011**, *12*, 2825-2830. DOI: 10.48550/arXiv.1201.0490.